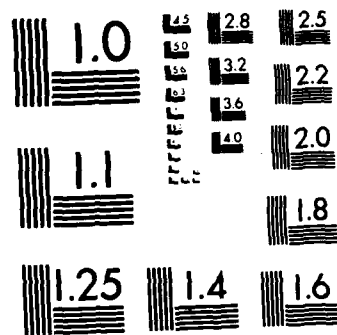| | 1.0 | | 2.8 | 2.5 |
			3.2	2.2
			3.6	
			4.0	2.0
	1.1			1.8
	1.25	1.4		1.6

MICROCOPY RESOLUTION TEST CHART

NATIONAL BUREAU OF STANDARDS-1963-A

AD-A134514

A Comparison of SMMR and Airborne Microwave Measurements During GOASEX

BALLARD E. TROY, JR., JAMES P. HOLLINGER, AND ROBERT C. LO

Space Sensing Applications Branch
Aerospace Systems Division

September 30, 1983

DTIC FILE COPY

DTIC
ELECTE
NOV 8 1983

A

NAVAL RESEARCH LABORATORY
Washington, D.C.

83 11 08 008

REPORT DOCUMENTATION PAGE		READ INSTRUCTIONS BEFORE COMPLETING FORM
1. REPORT NUMBER NRL Memorandum Report 5169	2. GOVT ACCESSION NO. AD-A134514	3. RECIPIENT'S CATALOG NUMBER
4. TITLE (and Subtitle) A COMPARISON OF SMMR AND AIRBORNE MICROWAVE MEASUREMENTS DURING GOASEX		5. TYPE OF REPORT & PERIOD COVERED Final report on one phase of an NRL problem.
		6. PERFORMING ORG. REPORT NUMBER
7. AUTHOR(s) Ballard E. Troy, Jr., James P. Hollinger, and Robert C. Lo		8. CONTRACT OR GRANT NUMBER(s)
9. PERFORMING ORGANIZATION NAME AND ADDRESS Naval Research Laboratory Washington, DC 20375		10. PROGRAM ELEMENT, PROJECT, TASK AREA & WORK UNIT NUMBERS 35160; SPW 0524-CC; 79-1543-0-0
11. CONTROLLING OFFICE NAME AND ADDRESS Naval Space Systems Activity Los Angeles, CA 90009		12. REPORT DATE September 30, 1983
		13. NUMBER OF PAGES 48
14. MONITORING AGENCY NAME & ADDRESS(if different from Controlling Office)		15. SECURITY CLASS. (of this report) UNCLASSIFIED
		15a. DECLASSIFICATION/DOWNGRADING SCHEDULE

16. DISTRIBUTION STATEMENT (of this Report)

Approved for public release; distribution unlimited.

17. DISTRIBUTION STATEMENT (of the abstract entered in Block 20, if different from Report)

18. SUPPLEMENTARY NOTES

19. KEY WORDS (Continue on reverse side if necessary and identify by block number)

Remote sensing	GOASEX
Microwave radiometry	Passive
SMMR	Ocean
SEASAT	

20. ABSTRACT (Continue on reverse side if necessary and identify by block number)

The Naval Research Laboratory (NRL) measured the microwave brightness temperature (T_B) of the open ocean during September 1978 in a series of aircraft flights as part of the Gulf of Alaska Experiment (GOASEX). The purpose of GOASEX was to evaluate the performance of the remote sensors aboard SEASAT. One of the SEASAT sensors was the Scanning Multichannel Microwave Radiometer (SMMR), which measured

(Continues)

DD FORM 1473 EDITION OF 1 NOV 65 IS OBSOLETE
1 JAN 73
S/N 0102-014-6601

20. ABSTRACT (Continued)

-the ocean T_B at five microwave frequencies from 6.6 to 37 GHz. The NRL flights were performed to validate the SMMR microwave measurements.

The aircraft measurements and the SMMR measurements were made at different but overlapping frequency ranges, and slightly different incidence angles. In order to compare the two sets of measurements, an estimate of the SMMR T_B's at satellite altitude is derived from the aircraft measurements. Corrections for differences in altitude, frequency and incidence angle are made by the NRL Environmental Model, which is used to compute the atmospheric microwave parameters necessary for the correction based on the meteorological conditions at the time of the measurements.

The results show that the SMMR T_B's are in error at most frequencies, being generally smaller than the aircraft T_B's. Biases which must be added to the SMMR T_B's to bring them into agreement with the aircraft T_B's are approximately the same as empirically derived biases for correcting the SMMR T_B's prior to using them in geophysical algorithms.

CONTENTS

iii

A COMPARISON OF SMMR AND AIRBORNE
MICROWAVE MEASUREMENTS
DURING GOASEX

1.0 INTRODUCTION

The Gulf of Alaska Experiment (GOASEX) was a joint NASA/NOAA
effort conducted to evaluate the performance of the ocean
surveillance satellite, SEASAT. GOASEX was conducted from 28
August to 26 September 1978, shortly after the SEASAT launch on
26 June 1978. Surface and near-surface measurements were made
by a variety of instruments on aircraft, ships, and buoys for
comparison with measurements made by the remote sensors aboard
the satellite. The Naval Research Laboratory RP-3A, which
carried a set of downward-looking radiometers to measure the
microwave emission of the open ocean, participated in the
experiment.

The SEASAT remote sensing instruments were designed to
determine various oceanic and atmospheric parameters on a global
all-weather basis. In the case of the Scanning Multichannel
Microwave Radiometer (SMMR), they are sea surface temperature,
wind speed, and atmospheric liquid water and water vapor. These
parameters are determined in a multi-step process. First, the
raw SMMR output measurements are converted to the absolute power
received by the radiometer, the antenna temperature, T_A. Then
T_A is corrected for the directional effects and antenna losses
to obtain the absolute radiation from the scene being viewed by
the radiometer, the brightness temperature, T_B. Although T_B is
a weighted average over the instrument parameters of bandwidth
and spatial response, it is otherwise independent of the sensor
and is a unique measurement of the scene which depends only on
the physical properties of the scene. The last step in the
process is the conversion of T_B to the desired geophysical
parameters by empirically-theoretically determined algorithms.

The most obvious method to evaluate the overall instrument performance is to see how accurately it determines the geophysical parameters which it was designed to measure. Sea surface temperature, for example, can be measured in-situ and compared to the corresponding values obtained from SMMR. Instrument evaluation by this method involves not only the instrument itself, but also the algorithms used to derive the parameters from the instrument measurements. A more direct method of validating the instrument alone is to validate the input to the algorithms, i.e., the brightness temperature. Of the quantities computed during the data analysis process of converting raw measurements into geophysical parameters, T_B is the first one which is independent of the instrument and therefore subject to external verification.

This verification is provided for SMMR by the NRL aircraft experiment: radiometers aboard the aircraft measure the microwave brightness temperature of the ocean surface for comparison with the corresponding values measured by SMMR. The performance and results of the experiment are described in this report.

2.0 EXPERIMENT DESCRIPTION

2.1 AIRCRAFT

Four passive microwave radiometers were mounted on a pallet in the lower fairing of the aircraft. Figure 1 shows the RP-3A aircraft; the fairing is immediately behind the front landing gear. One of the radiometers was dual-frequency, measuring the horizontally (H) polarized radiation at 22.2 GHz and the vertically (V) polarized radiation at 31.3 GHz. The other three radiometers were single-frequency, measuring both H and V at 6.15, 14.3, and 19.3 GHz. The pallet could be tilted during flight so that the radiometers could view either in the nadir direction or at 50 degrees off nadir.
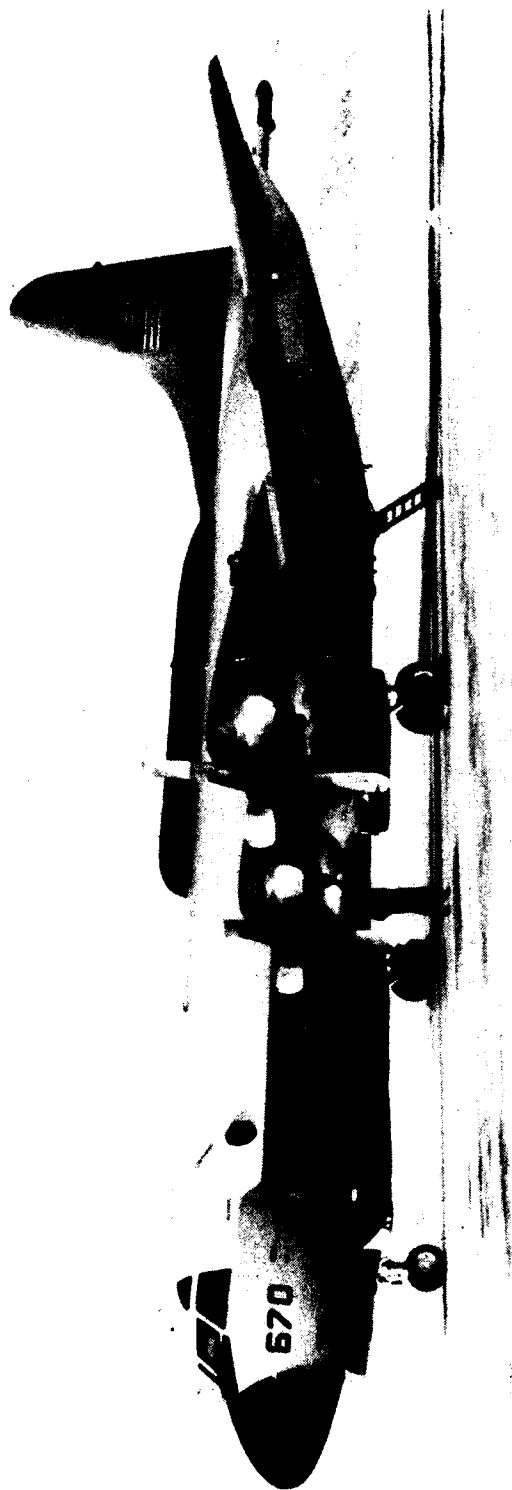
R-983

Figure 1. The NRL research aircraft RP-3A 149670. The microwave radiometers are located in the lower fairing behind the front landing gear.

All of the radiometers were Dicke switched. The 6.15 and 14.3 GHz radiometers used tunnel diode amplifiers covering the bands 5.9 to 6.4 and 13.5 to 15.5 GHz. The other three were crystal-mixer-superheterodyne receivers with local oscillators at 19.3, 22.2, and 31.4 GHz and IF amplifiers with band passes of 10 to 300 MHz. The 22/31 GHz radiometer used a corrugated horn with beam widths of 8.4° and 7.9° and main beam efficiencies of 97.5% and 98.2%. All the others used horn lens antennas with beam widths and beam efficiencies of 7.9° and 80%, 7.9° and 80%, and 8.0° and 87% at 6.15, 14.3, and 19.3 GHz, respectively.

In addition to the radiometers, the aircraft carried a complement of instruments to make supporting meteorological and environmental measurements. Wind speed and direction at aircraft altitude were computed by the aircraft inertial navigation system (INS). Sea surface temperature was measured by a Barnes infrared radiometer. Atmospheric pressure, outside air temperature (OAT), and dew point were measured at aircraft altitude. The OAT lapse rate and water vapor scale height were subsequently determined from these data taken during aircraft descent. Whenever possible, environmental parameters measured by aircraft instruments were checked against independent measurements from ships and buoys.

2.2 SMMR

The SEASAT SMMR instrument is an imaging microwave radiometer measuring both V and H polarized radiation at the five frequencies 6.6, 10.7, 18, 21, and 37 GHz. Half-power beamwidth varies from 0.9° at 37 GHz to 4.5° at 6.6 GHz. The nadir angle of 42° at the 794 km satellite altitude results in an incidence angle of 48.8° at the earth's surface. A mechanically scanning reflector sweeps the line-of-sight back and forth across a swath of 600 km width. One sweep across the swath takes two seconds, during which 55 data samples are taken at 37 GHz, 14 samples at 6.6 GHz, and 27 samples at each of the other three frequencies. The 18 GHz data points during several sweeps are shown in

4

Figure 2, illustrating the arc-shaped sweep and the region of
data coverage. Also shown are the resampled grid points at
which the Jet Propulsion Laboratory (JPL) determines interpolated
T_B's (Njoku et al., 1980a). A detailed description of the SMMR
instrument and its method of operation has been published by
Njoku et al. (1980b).

2.3 FLIGHT DESCRIPTION

Five GOASEX flights were conducted by the RP-3A during the
period 19-27 September 1978. There were equipment problems on
the flight of 19 September, but good data were obtained on the
flights of 21, 22, 25, and 27 September. This report is based
on the data from those four flights.

The corresponding flight paths are shown in Figures 3-6.
The first two flights were made during ascending satellite
passes, and the second two during descending passes. Each
flight began with a transit at 20,000 feet altitude from the
mainland to the OSS OCEANOGRAPHER. Observations began during a
spiral descent over the OCEANOGRAPHER to a 500 ft. altitude.
Next, a star pattern was flown at 500 ft. in the vicinity of the
OCEANOGRAPHER. The RP-3A then flew a leg out to the subsatellite
track, and a leg along the track completing the measurements.

The radiometer outputs were recorded for several minutes
alternately at 0° and at 50° incidence angle during flight by
rotating the pallet, so that several minutes passed between
successive T_B determinations. The aircraft altitude varied in
steps from 500 ft. to a maximum of 5000 ft. during the two legs,
with the flight generally beginning and ending at 500 ft. The
altitude for each leg is shown in Figures 3-6. The total measure-
ment period lasted approximately 3-4 hours. Each T_B determination
corresponds to one minute or more of continuous observation,
during which T_B generally varied by less than 2K. Changes in T_B
may be attributed to changes in environmental conditions, such
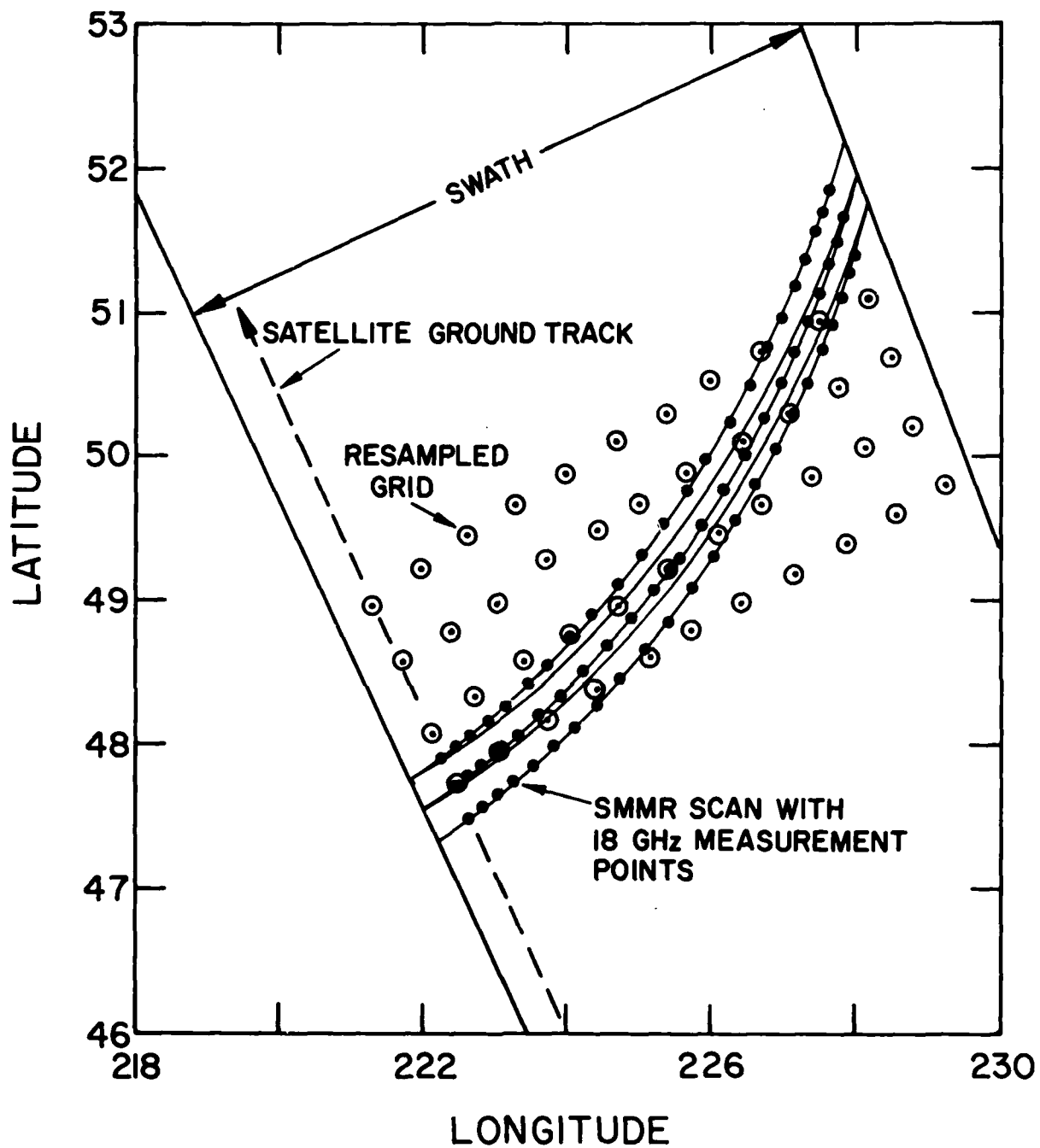as cloud cover, surface wind speed, or aircraft altitude.

5

Figure 2. SMMR data swath, illustrating the scans, individual 18 GHz measurements points, and JPL resampled grid points.
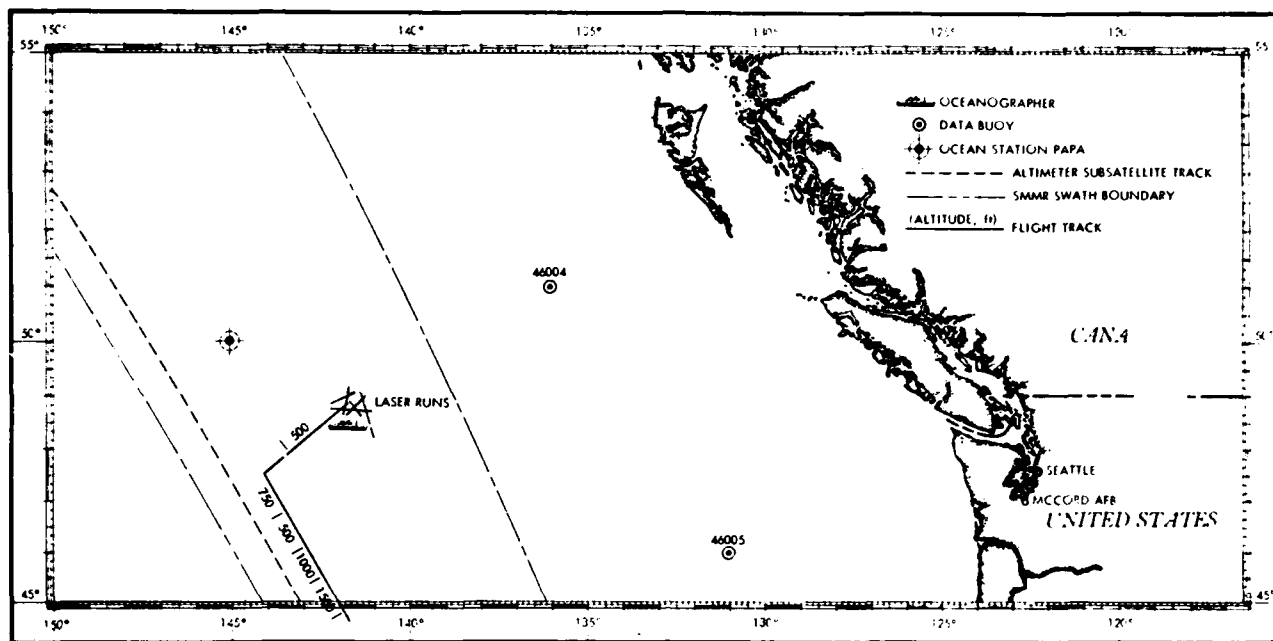
6

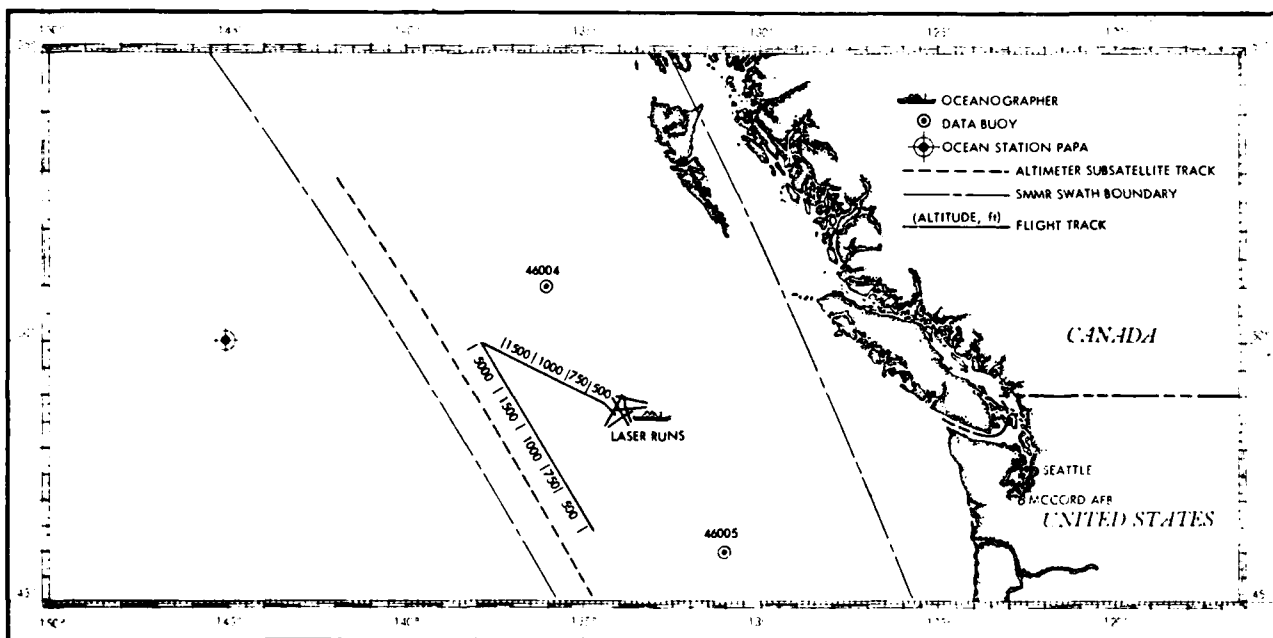**Figure 3.** NRL RP-3A flight track on 21 September 1978.

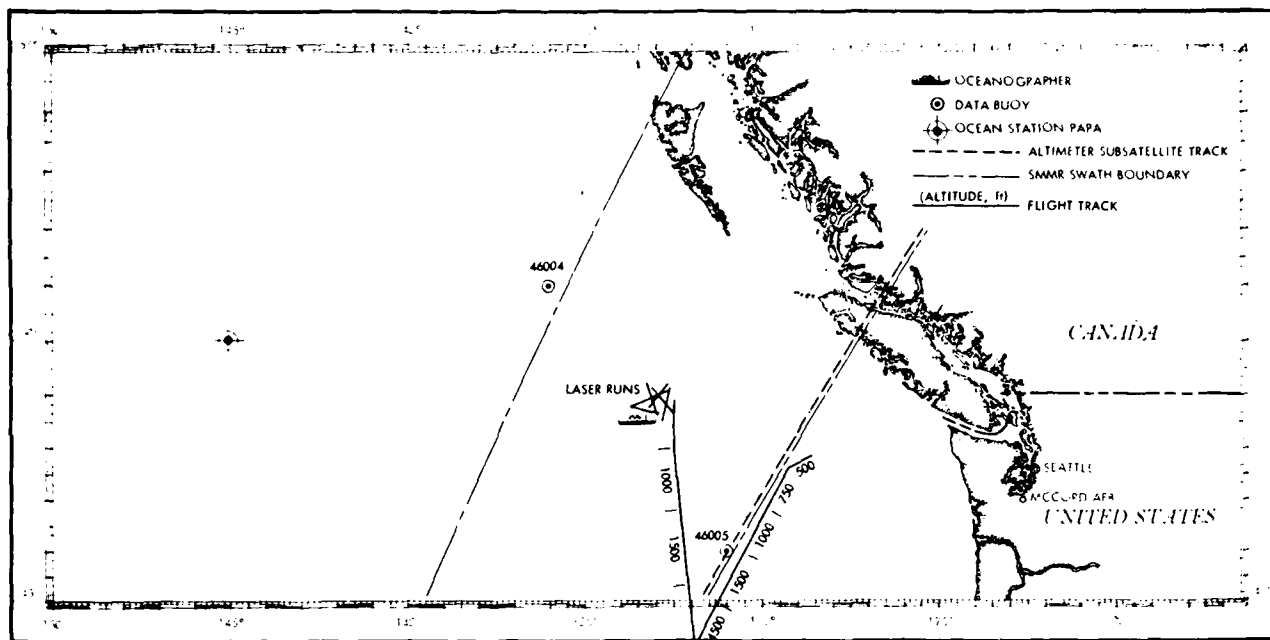**Figure 4.** NRL RP-3A flight track on 22 September 1978.

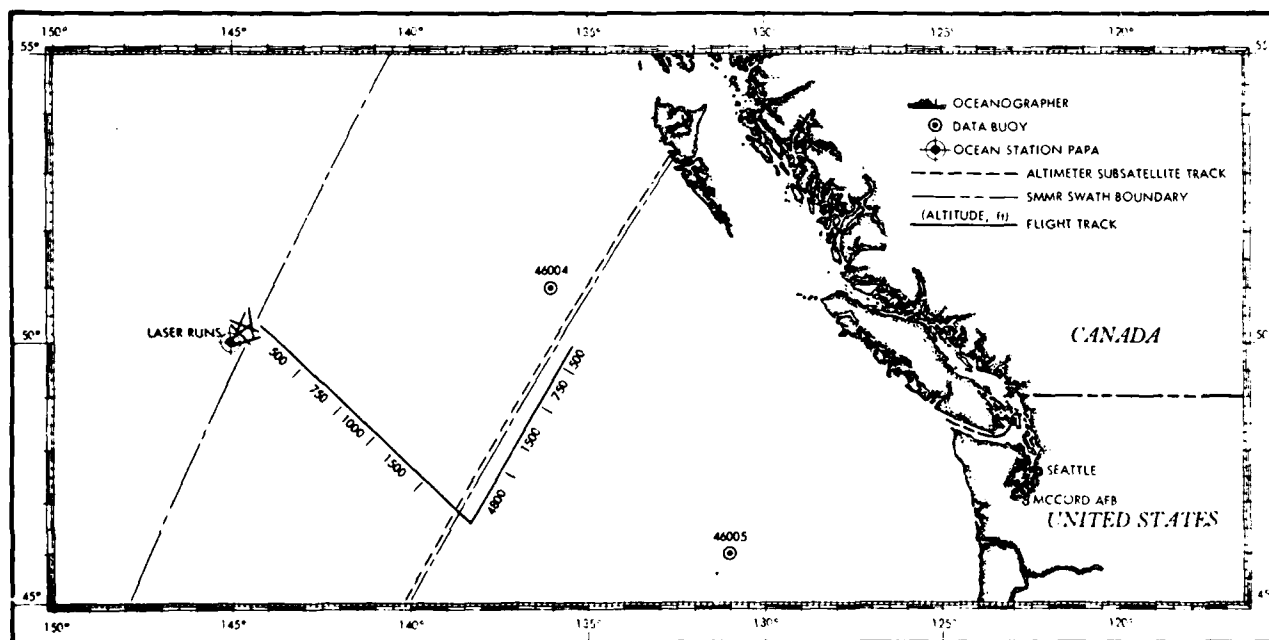Figure 5. NRL RP-3A flight track on 25 September 1978.

Figure 6. NRL RP-3A flight track on 27 September 1978.

8

3.0 DATA ANALYSIS

3.1 DATA ANALYSIS OUTLINE

The final product of this report is a comparison of the brightness temperatures measured by SMMR and by the aircraft radiometers. Since the two sets of measurements were taken at different altitudes, overlapping but slightly different frequencies, and slightly different nadir angles, several calculations must be made after the T_B's are derived before a direct comparison can be undertaken.

There are four main steps in the data analysis routine performed by NRL. First, brightness temperatures are derived at satellite altitude and frequencies from SMMR antenna temperatures provided to NRL by JPL. Second, brightness temperatures at aircraft altitude and frequencies are computed from the flight measurements. Third, the NRL environmental model computer program (Wisler and Hollinger, 1977) is used to compute the expected T_B's, atmospheric loss factors and emitted atmospheric radiation for all frequencies, altitudes, and incidence angles for the existing environmental conditions. Finally, estimates for the SMMR T_B's are derived from the aircraft T_B's, using the environmental model calculations to correct for differences in frequencies, altitude, and incidence angle between the SMMR and aircraft measurements. These estimated SMMR T_B's based on the aircraft measurements are then compared with the SMMR T_B's measured at SEASAT altitude.

The four data analysis steps are described in detail in the following sections.

3.2 DERIVATION OF SMMR BRIGHTNESS TEMPERATURE

SMMR brightness temperatures at satellite altitude are determined from antenna temperatures supplied by JPL on Sensor Data Record (SDR) tapes. The SDR tapes contain pairs of T_A values for all frequencies, and earth location information for

the corresponding arc-shaped scans (see Figure 2). Computations made at NRL pair the T_A valus for H and V polarization and determine the corresponding latitude, longitude, and polarization angle, α. The paired T_A values are then converted to T_B by JPL's interim Antenna Pattern Correction (APC) method rather than by their final detailed and extensive APC method (Njoku et al., 1980a). The interim method assumes a relatively homogeneous microwave scene, such as the open ocean, and uses negligible computer time compared to the final method. In addition to the SDR tapes for the four aircraft flight days, JPL has provided NRL another tape with SMMR T_B values computed at JPL by both the interim APC method and the final APC method for one flight day, 22 September. Similar data were not provided for the other three flight days because of the large amounts of computer time involved. These JPL T_B's are used to check the accuracy of the T_B values computed at NRL from the JPL SDR tapes by the JPL interim APC method. First, the NRL T_B's are compared to the JPL T_B's computed by the interim APC method. This comparison necessitates some averaging of the NRL T_B's, since the JPL T_B's are on the gridded format and the NRL values derived from the SDR tapes are more densely packed along the arc-shaped SMMR sweep (see Figure 2). Next, the NRL T_B's are compared to the JPL T_B's computed by the final extensive APC method, and a small bias between the two T_B's sets is determined for each frequency and polarization. The bias is then used to correct the NRL T_B values. This method insures that the NRL-computed SMMR T_B's are in agreement with the T_B's computed at JPL by the most accurate available technique. Also, direct conversion of the SDR tape T_A's to T_B's results in a greater density of data points than in the JPL gridded format, and thus allows the selection of SMMR data points closer to the aircraft measurement locations.

A brief description of the interim APC method is now given. First, the antenna temperatures are corrected for the cold space contribution by

10

$$T_A' = \frac{T_A - 2.7\lambda}{1 - \lambda},$$

(1)

where λ is the fractional contribution to T_A due to the portion of the antenna viewing the 2.7K space background. Values of λ, provided by JPL, are listed in Table 1.

Next, T_B is derived from T_A'. If T_{AH}' and T_{AV}' are the horizontal and vertical antenna temperatures, and $T_{B\phi}$ and $T_{B\theta}$ the horizontal and vertical brightness temperatures, then they are related by

$$T_{AH}' = G_{H\theta} T_{B\theta} + G_{H\phi} T_{B\phi}$$

$$T_{AV}' = G_{V\theta} T_{B\theta} + G_{V\phi} T_{B\phi},$$

(2)

where

$$G_{V\theta} = g_{V\theta} \cos^2\alpha + g_{V\phi} \sin^2\alpha + \text{TERM V}$$

$$G_{V\phi} = g_{V\phi} \cos^2\alpha + g_{V\theta} \sin^2\alpha - \text{TERM V}$$

$$G_{H\theta} = g_{H\theta} \cos^2\alpha + g_{H\phi} \sin^2\alpha + \text{TERM H}$$

(3)

$$G_{H\phi} = g_{H\phi} \cos^2\alpha + g_{H\theta} \sin^2\alpha - \text{TERM H}$$

$$\text{TERM V} = \sqrt{g_{V\theta} \, g_{V\phi} \, \sin^2\alpha \, \cos \beta_V}$$

$$\text{TERM H} = \sqrt{g_{H\theta} \, g_{H\phi} \, \sin^2\alpha \, \cos \beta_H}$$

The above equations are derived from the method of Claassen and Fung (1974), and account for the cross-polarization correction due to the instrumental polarization rotation with scan angle (through $\sin^2\alpha$ and $\cos^2\alpha$), cross-polarization (through the g's) and cross-track gradients (through $\cos \beta$). The g's are integrated antenna pattern co- and cross-polarization terms and are given in Table 1. β is the relative phase between polarization components. Values of $\cos \beta$ are derived empirically at JPL by averaging 300 minutes of data and are also given in Table 1.

11

TABLE 1

SMMR APC Parameters

	λ	g_θ	g_ϕ	$\cos\beta$	Bias,K	RMS,K
6H	.056668	.0617	.9383	.23	0.7	1.0
6V	.070514	.9386	.0614	-.04	4.3	1.2
10.7H	.042106	.0636	.9364	.03	2.1	0.5
10.7V	.046942	.9427	.0573	.06	3.5	0.9
18H	.026469	.0301	.9699	.21	2.1	1.0
18V	.034169	.9663	.0337	-.24	3.9	0.9
21H	.038395	.0444	.9556	.33	2.0	0.8
21V	.032887	.9603	.0397	-.10	3.3	1.0
37H	.012175	.0367	.9633	.08	1.7	1.1
37V	.015922	.9568	.0432	.09	2.4	0.6

12

Equations (2) are inverted to obtain $T_{B\theta}$ and $T_{B\phi}$ from T'_{AV} and T'_{AH}. Note that since

$$g_{V\theta} + g_{V\phi} = 1 \quad \text{and} \quad g_{H\theta} + g_{H\phi} = 1,$$

then

$$G_{V\theta} + G_{V\phi} = 1 \quad \text{and} \quad G_{H\theta} + G_{H\phi} = 1.$$

As a result, the inverted equations (2) may be expressed as

$$T_{B\theta} = \frac{G_{H\phi}T'_{AV} - G_{V\phi}T'_{AH}}{G_{H\phi} - G_{V\phi}}$$

$$(4)$$

$$T_{B\phi} = \frac{G_{V\theta}T'_{AH} - G_{H\theta}T'_{AV}}{G_{V\theta} - G_{H\theta}}.$$

The brightness temperatures computed from equation (4) represent the JPL interim APC method. A comparison of the resulting T_B values computed at NRL from the SDR tape T_A's and the interim T_B values provided by JPL shows that the two sets are quite close for all frequencies. The average RMS difference is 0.7K, showing that the interim APC method is being correctly applied at NRL. On the other hand, the final JPL T_B values are a few degrees lower than the corresponding interim T_B values on the JPL-provided tape for 22 September. The difference between the T_B's computed by the final APC method and those computed by the interim APC method has been noted by JPL (Christensen, 1981). Therefore, a bias is derived for each frequency and polarization between the NRL T_B's and the final JPL T_B's by averaging both sets over the entire flight area for 22 September, and is subsequently subtracted from the individual NRL T_B values. The biases are listed in Table 1. Figures 7-11 show the resulting NRL values and the final JPL values for each SMMR frequency across the SMMR swath. Table 1 lists the RMS deviation between the two sets for each channel. The low RMS values of approximately 1K indicate that the SMMR T_B values computed at NRL with the interim APC method and used in this report are within one degree of the values computed by JPL using the final APC method.
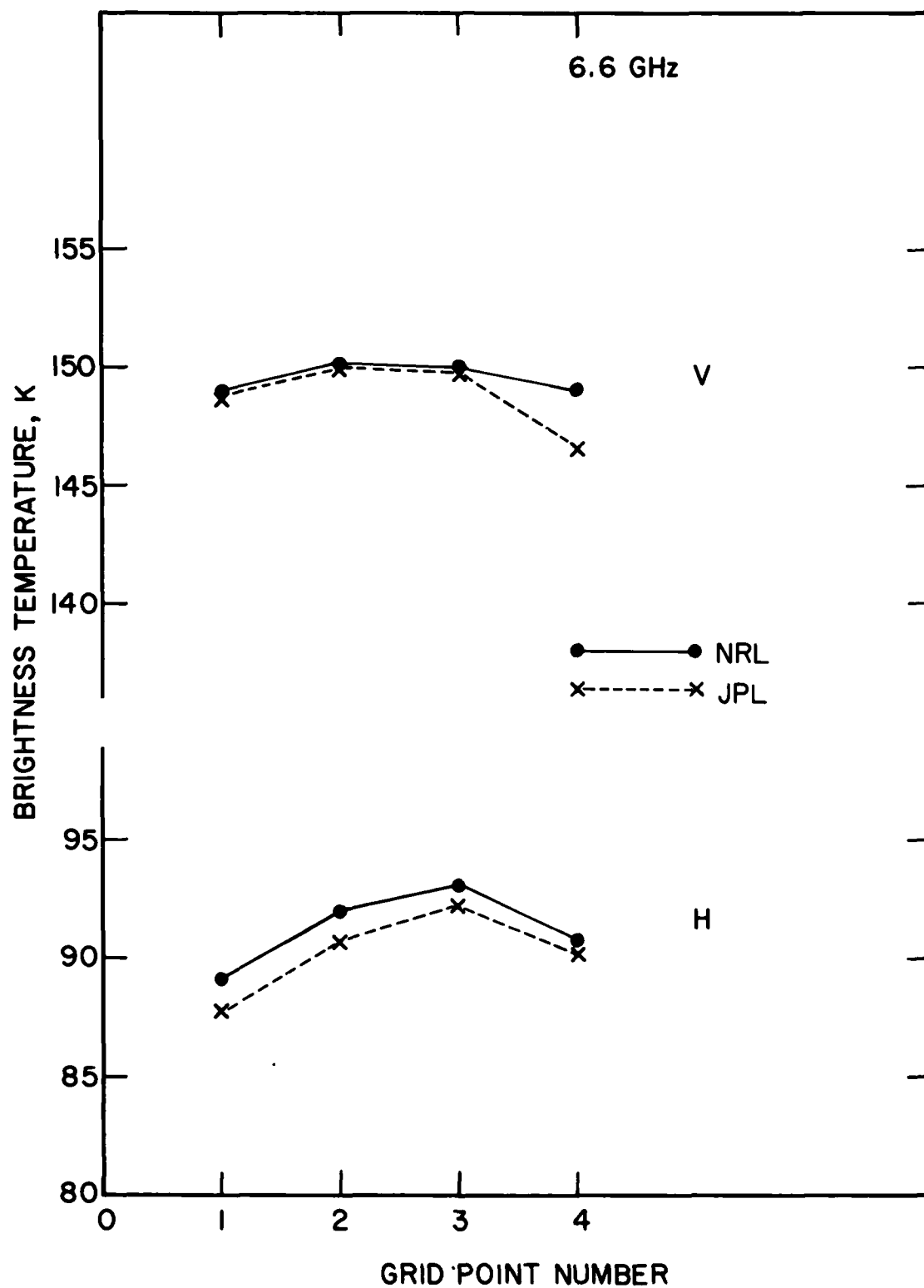
13

Figure 7. A comparison of 6.6 GHz SMMR brightness temperatures derived by JPL and NRL.
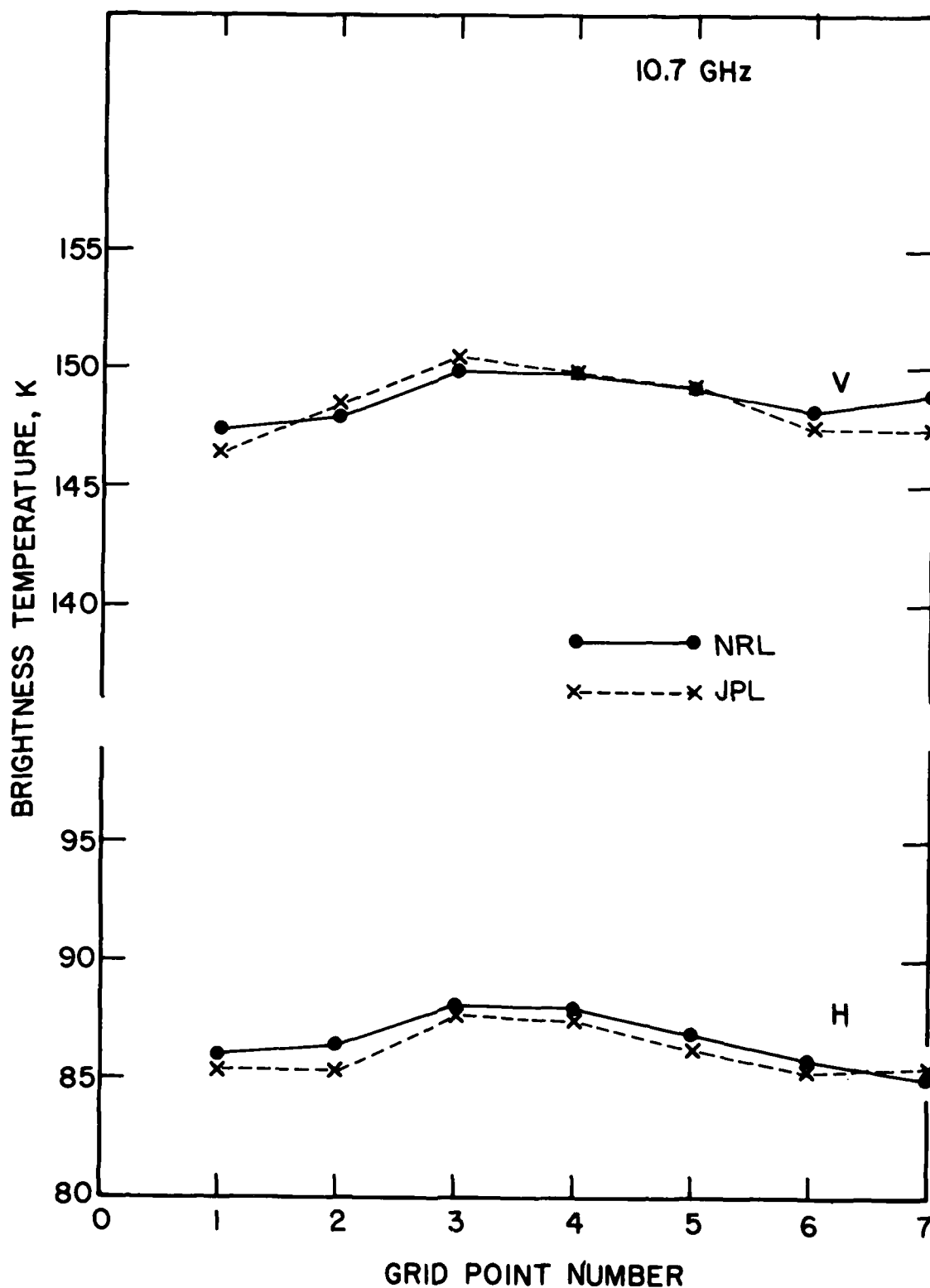
14

Figure 8. A comparison of 10.7 GHz SMMR brightness temperatures derived by JPL and by NRL.
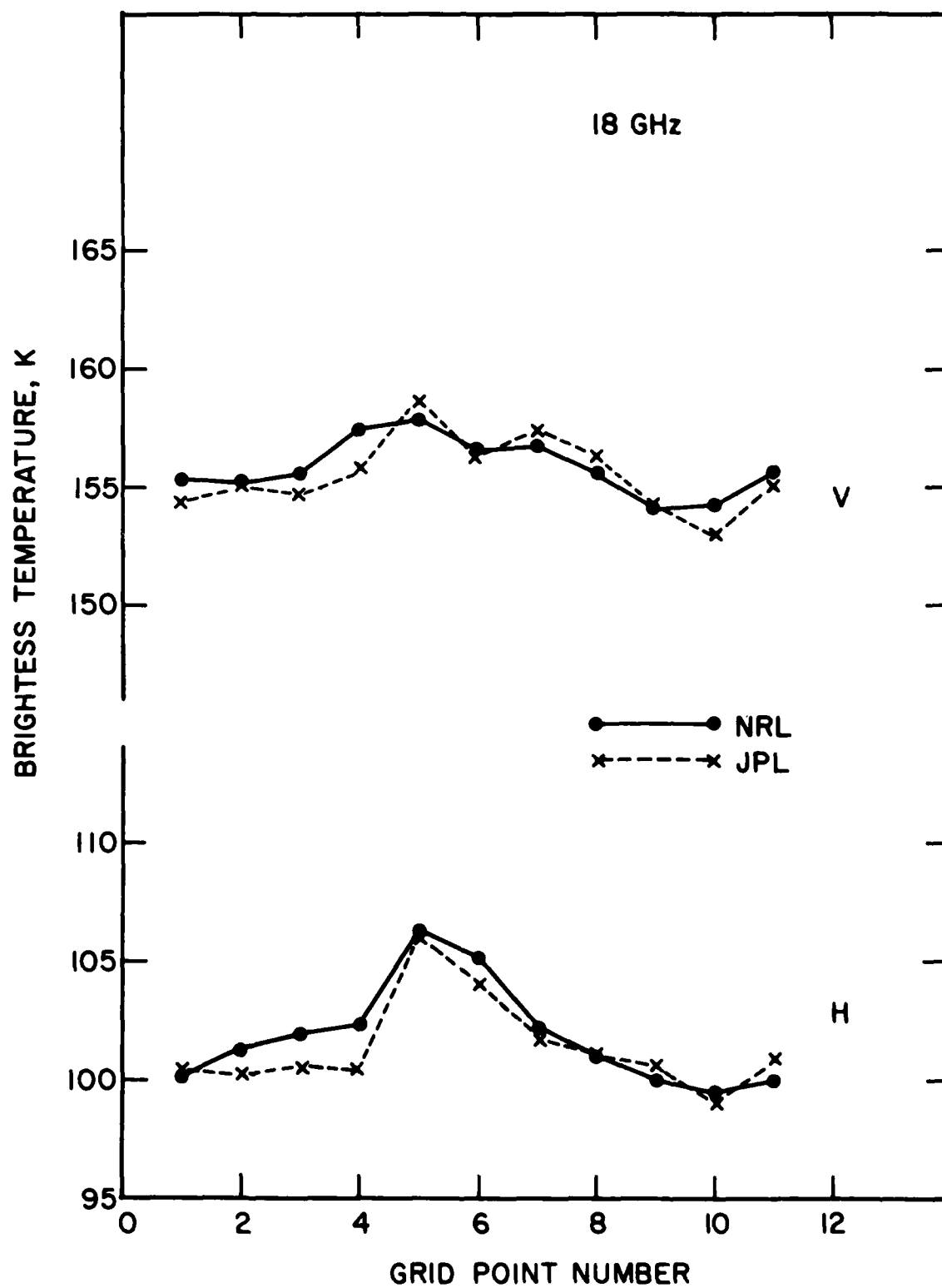
Figure 9. A comparison of 18 GHz SMMR brightness temperatures derived by JPL and by NRL.
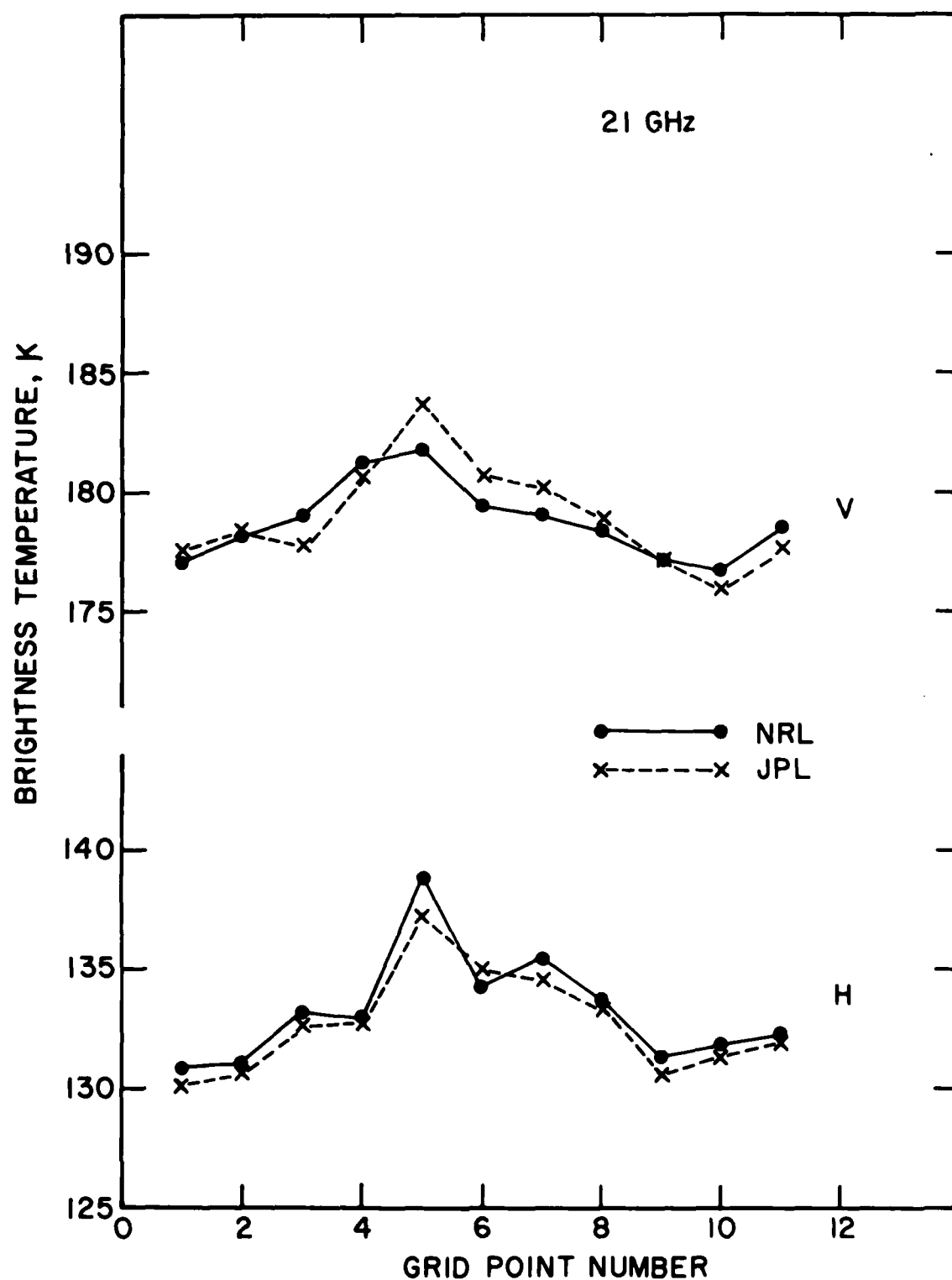
Figure 10. A comparison of 21 GHz SMMR brightness temperatures derived by JPL and by NRL.
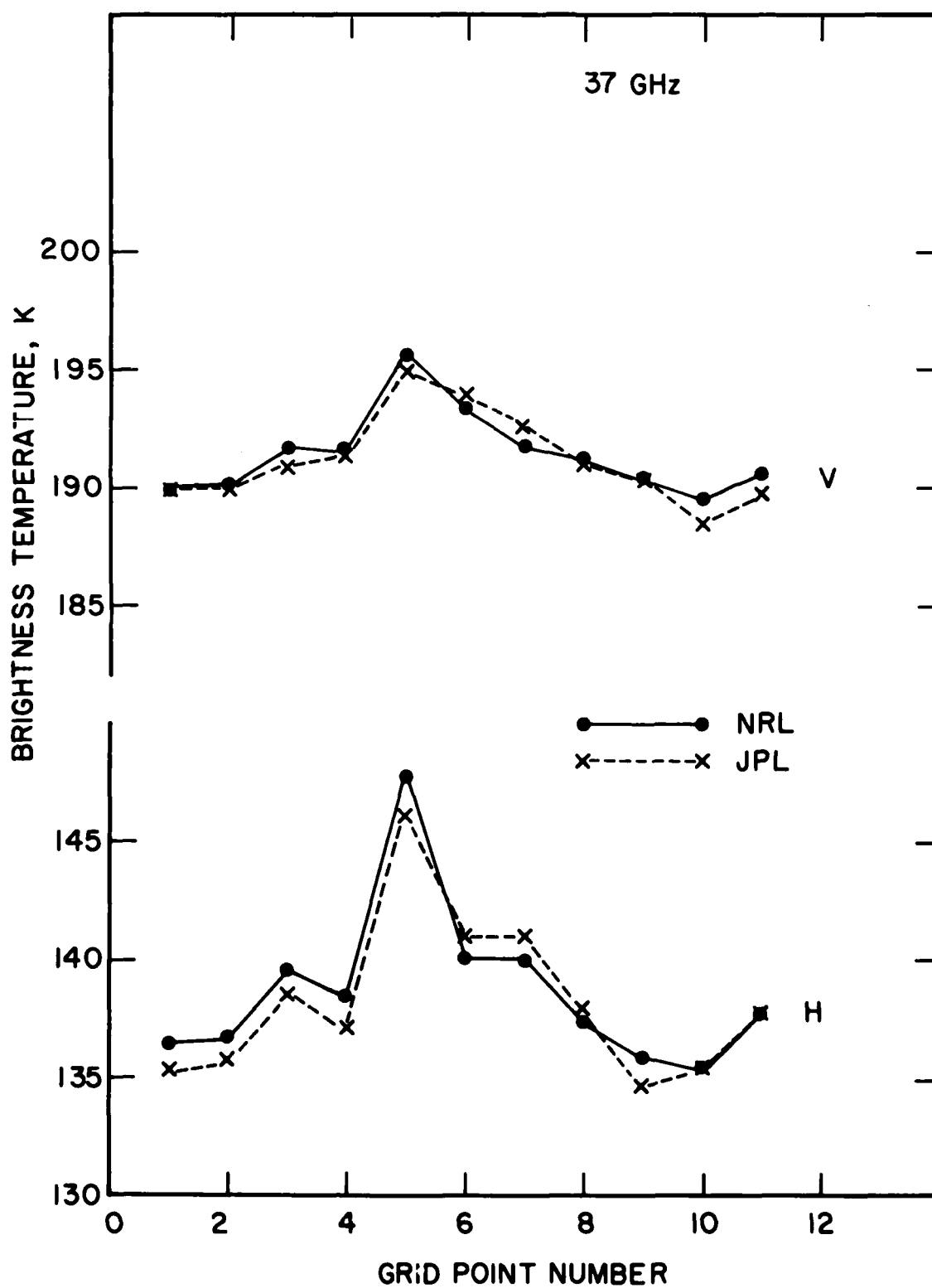
17

Figure 11.   A comparison of 37 GHz SMMR brightness temperatures derived by
              JPL and by NRL.

18

The bias values are applied to all four flights, which occur in the same area during a six-day period.

3.3 CALCULATION OF AIRCRAFT BRIGHTNESS TEMPERATURE

Both preflight and postflight calibrations of all aircraft radiometers were performed in the laboratory at NRL by immersing the antenna in black body enclosures. The preflight calibrations occurred within one week of the first flight, and the postflight calibrations within one week of the last flight. Two enclosures, spanning the range of measured brightness temperatures, were used: one at liquid nitrogen temperature of 79K for the low temperature point, and the other at ambient temperature of approximately 300K for the high-temperature point. The responses from the two enclosures are used to linearly interpolate the equivalent input temperature of an internal noise generator which is used as a secondary standard for inflight calibration.

Data are recorded during the aircraft flights on magnetic tape and on strip charts. Antenna readings are taken alternately at 0° and 50° incidence angle, with calibration readings being recorded between successive pairs of antenna readings. One antenna temperature value, T_A, is calculated for each antenna reading. T_A is then converted to brightness temperature, T_B, at aircraft altitude through antenna pattern corrections. The aircraft APC is simpler than the APC for SMMR, because the polarization angle α is always zero, and also because beamfilling is more complete at the low aircraft altitude. Conversion of T_A to T_B is accomplished by inversion of the equations

$$T_{AH} = g \, T_{B\theta} + (1-g) \, T_{B\emptyset}$$

$$T_{AV} = (1-g) \, T_{B\theta} + g \, T_{B\emptyset},$$

where g is the fraction of cross-polarized power. The values of g are computed from measured antenna patterns, and are approximately 0.090 for 6.15 and 14.3 GHz, 0.055 for 19.3 GHz, and negligibly small for 22.2 and 31.3 GHz.

19

The aircraft measurements result in a series of T_B determinations along the flight path and within the SMMR swath. The first T_B location is the star pattern area in the vicinity of the OCEANOGRAPHER. Several of these T_B measurements at 50° incidence angle are selected for comparison with the corresponding SMMR T_B values.

3.4 ENVIRONMENTAL MODEL CALCULATIONS

Direct comparison of the SEASAT SMMR T_B's and the aircraft T_B's is not possible, due to differences in frequency, incidence angle, and altitude. The aircraft measurements must be corrected to correspond to the SMMR frequencies, incidence angle, and altitude. Differences in frequency, angle, and altitude are accounted for by means of the NRL Environmental Model (Wisler and Hollinger, 1977). The model is used to calculate the necessary microwave quantities for modifying the measured aircraft T_B's. These quantities are: (1) the radiation emitted by the atmosphere between the satellite and aircraft altitudes, (2) the atmospheric loss factor between the two altitudes, and (3) the brightness temperature at aircraft altitude.

The Environmental Model calculations require the input of values for several atmospheric and oceanic parameters which largely determine the microwave brightness temperature, such as ocean surface temperature, atmospheric water vapor and liquid water content, low altitude wind speed, etc. These values are derived from measurements made during the experiment by aircraft, ships, and satellites. Table 2 lists the input parameters and their measurement sources. The OCEANOGRAPHER measurements are published in the GOASEX Surface Truth Data Inventory.

20

TABLE 2

Sources of Environmental Data

Environmental Parameter	Source
Surface Pressure	OCEANOGRAPHER
Air Temp. at Surface	OCEANOGRAPHER
Temp. Lapse Rate	Aircraft OAT During Descent
Absolute Humidity at Surface	OCEANOGRAPHER
Water Vapor Scale Height	Aircraft Data During Descent, Wentz Data
Clouds	OCEANOGRAPHER, Aircraft Observations, Satellite Imagery
Near-Surface Wind Speed	OCEANOGRAPHER, Aircraft INS
Sea Surface Temperature	OCEANOGRAPHER, Aircraft PRT-5

For each location along the aircraft flight path at which a SMMR/aircraft T_B comparison is to be made, environmental model calculations are performed using the best set of environmental parameter values for that particular location and time. Some of the parameters are measured or determined only once on each flight and are assumed constant for that flight. For example, the temperature lapse rate is determined from OAT measurements during aircraft descent from 20,000 ft. to 500 ft. altitude immediately prior to flying the star pattern.

The most difficult parameter to determine is cloud cover, i.e., atmospheric liquid water density versus altitude and earth location. To assist in this problem, GOES satellite IR images are obtained from the NOAA/Satellite Data Services Division, and the images are interpreted by a NOAA meteorologist to provide estimates of cloud type and thickness and of percent cloud cover. Figures 12-15 show the IR images for the four flights, together with the corresponding flight paths. Cloud cover in the flight area is generally heavier on the second two flights
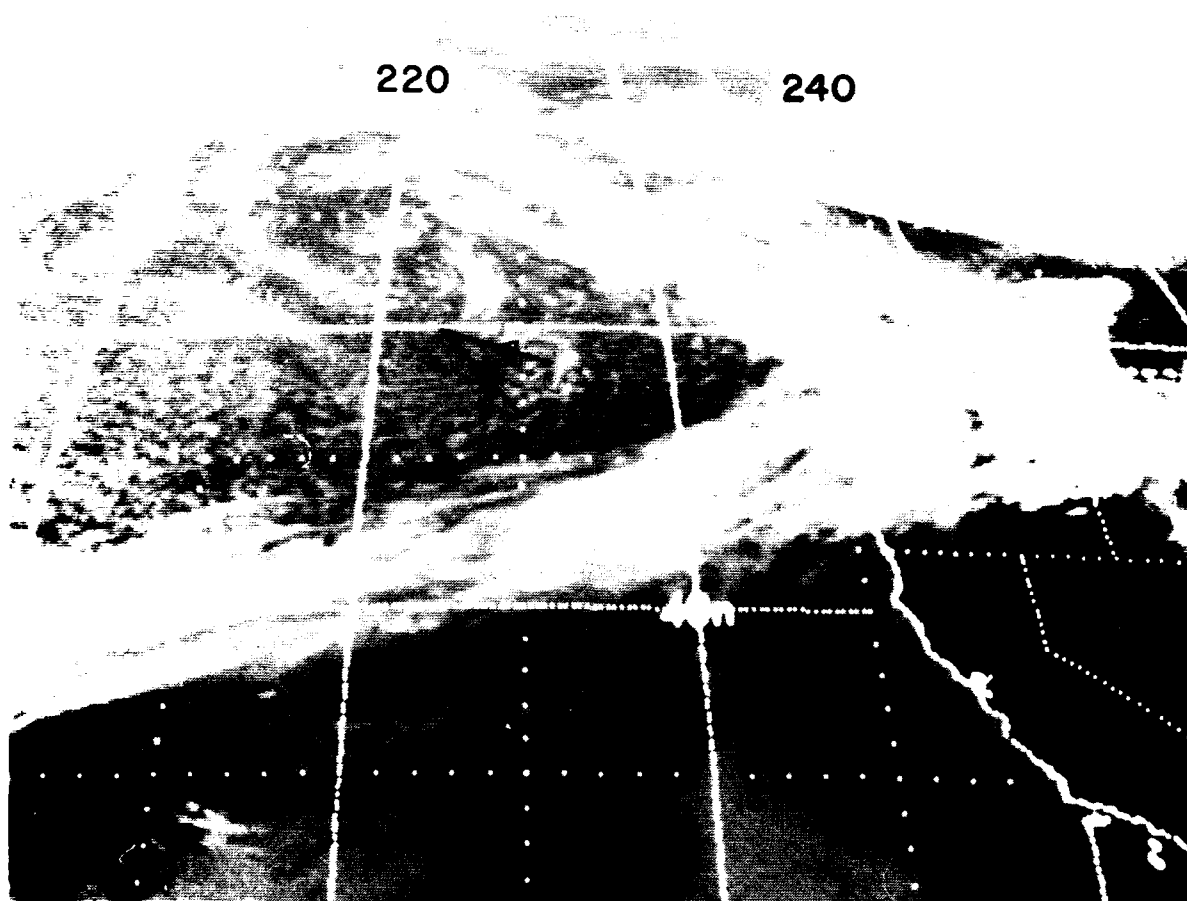
·Z 0006-1640 F

21 SEPT 1978

220   240
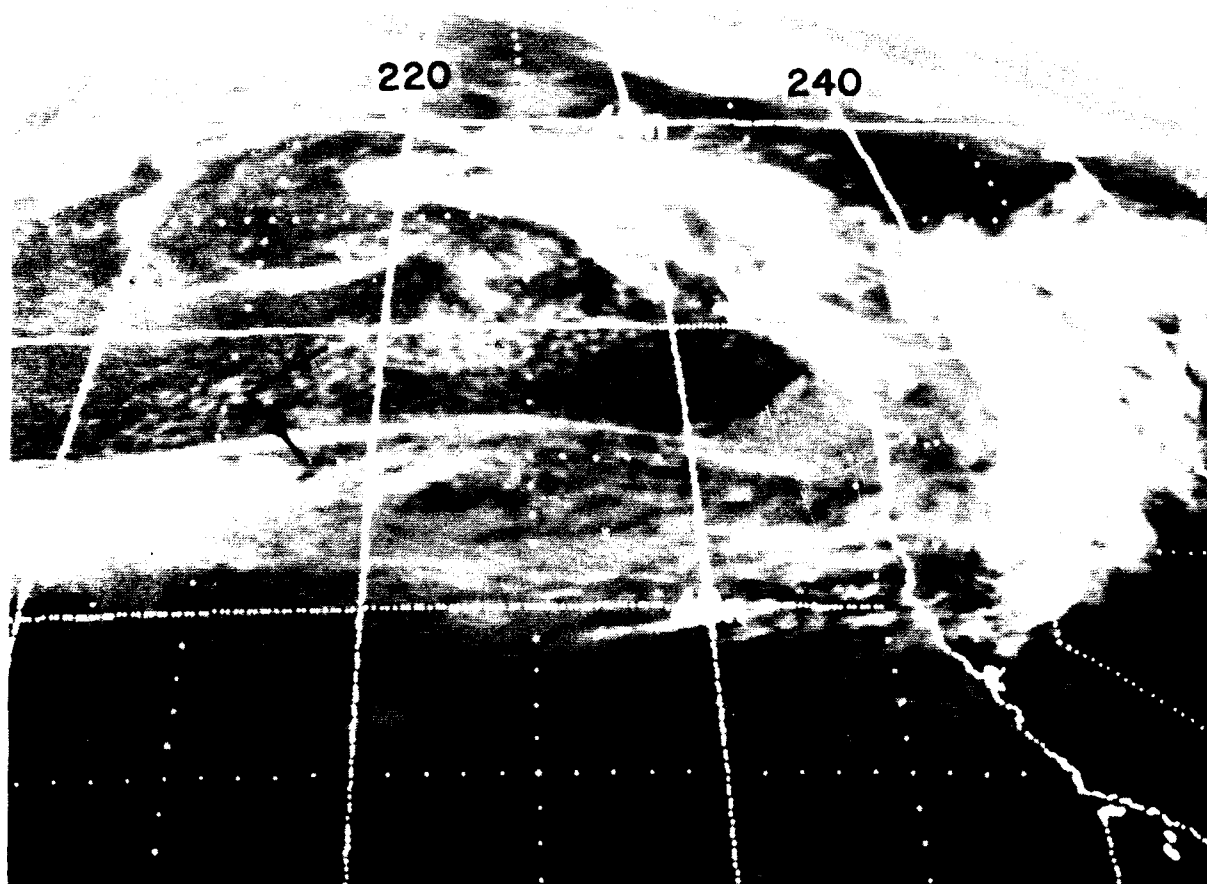
H-980

Figure 12.   GOES satellite infrared image of clouds in the GOASEX area on
21 September 1978 with the aircraft flight track.

·Z 0006-1640 F
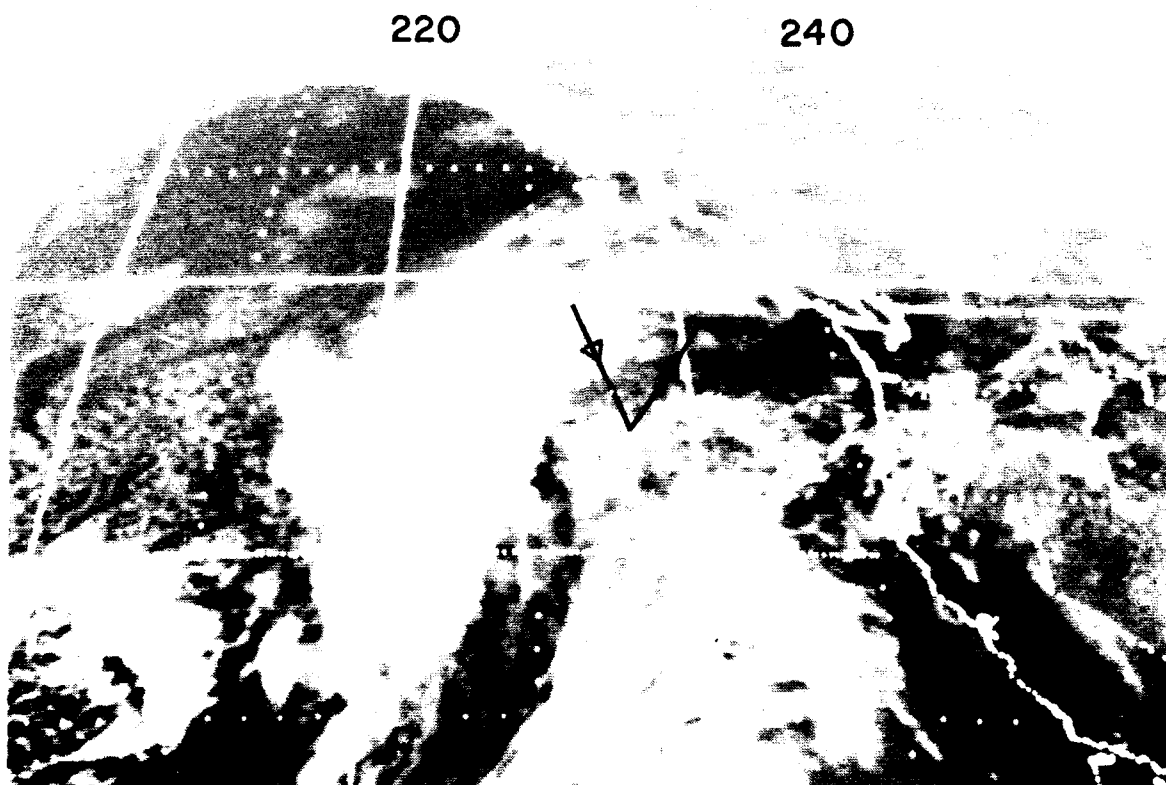
22 SEPT 1978

220   **240**

R-981

Figure 13.   GOES satellite infrared image of clouds in the GOASEX area on 22 September 1978 with the aircraft flight track.

23

Z 0006-1640 F

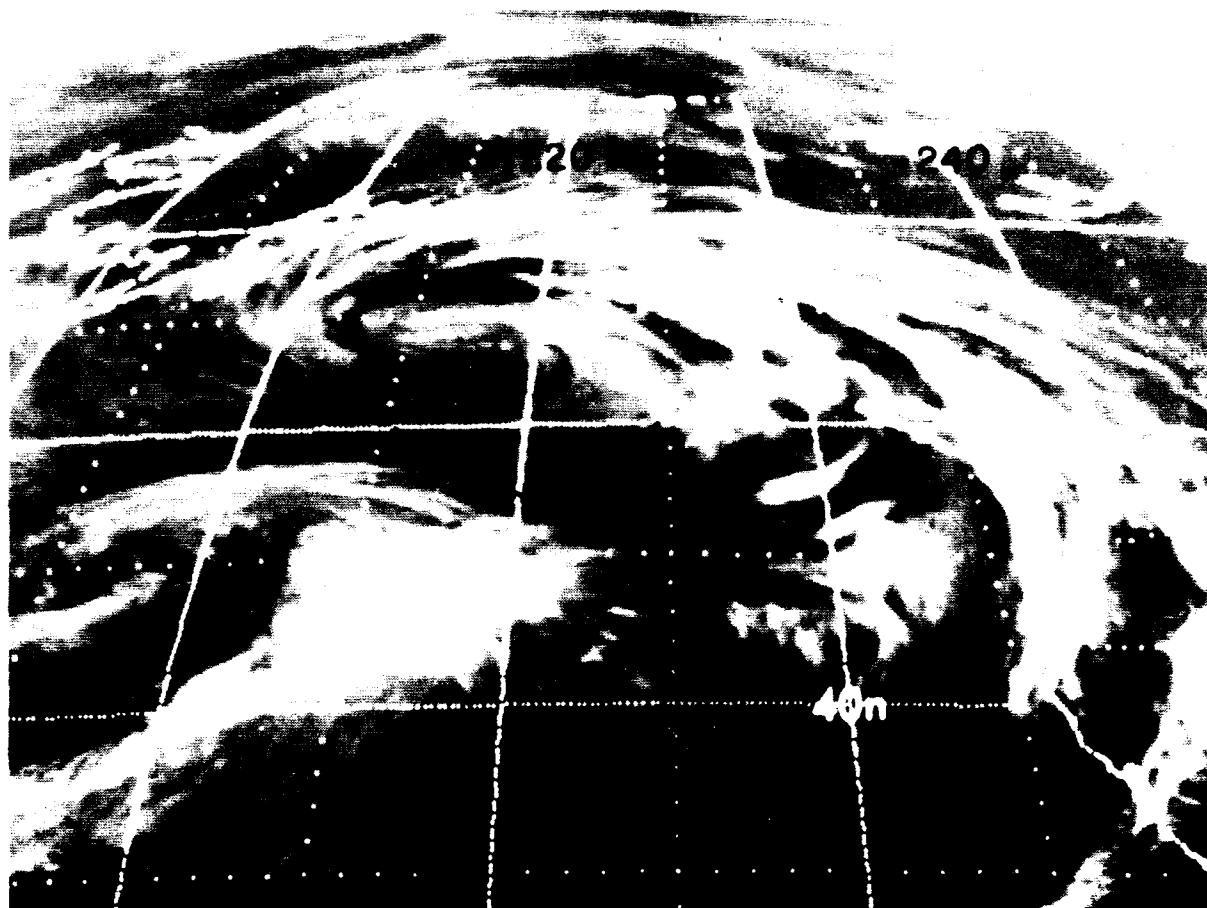25 SEPT 1978

220   240

R-982

Figure 14.   GOES satellite infrared image of clouds in the GOASEX area on
              25 September 1978 with the aircraft flight track.

-Z 0006-1640 F
27 SEPT 1978

R-979

Figure 15. GOES satellite infrared image of clouds in the GOASEX area on
27 September 1978 with the aircraft flight track.

than on the first two. The information from the IR images is used together with cloud information from the other sources to estimate the atmospheric liquid water content.

To obtain a valid brightness temperature comparison, data should be taken only from regions in which the meteorological conditions result in a relatively homogeneous microwave picture, free of strong local T_B gradients. Otherwise, the actual T_B within the small spot size of the low-altitude aircraft radiometers could be significantly different from the average T_B within the large spot size of the high-altitude SMMR radiometers. For the purpose of checking on the degree of T_B variability, microwave images of the GOASEX region are derived from the SMMR 37 GHz H measurements and are shown in Figures 16-19. The location of the flight path in each image indicates that the aircraft generally flew through quiet microwave regions with T_B < 165K. Regions of strong microwave variability and T_B > 180K correspond to heavy cloud areas seen in the IR images. One exception is that the areas of high T_B in the top of Figure 18 represent the Canadian landmass rather than clouds.

3.5 DERIVATION OF ESTIMATED SMMR BRIGHTNESS TEMPERATURE

Estimates of the SMMR T_B's, based on the measured aircraft T_B's, are derived for comparison with the measured SMMR T_B's according to the following scheme.

A. _Look Angle_ - The measured aircraft T_B's are extrapolated in look angle from the 50° aircraft angle to the 48.8^O SMMR angle. An estimate $E(F_A, 48.8, low)$ of T_B at aircraft frequency F_A, 48.8^O incidence angle and aircraft altitude is derived from the corresponding measured value $M(F_A, 50, low)$ by calculating the difference in T_B due to the angular change and adding the difference to the measured value:

$$E(F_A,48.8,low) = M(F_A,50,low) + [C(F_A,48.8,low) - C(F_A,50,low)] \quad (5)$$
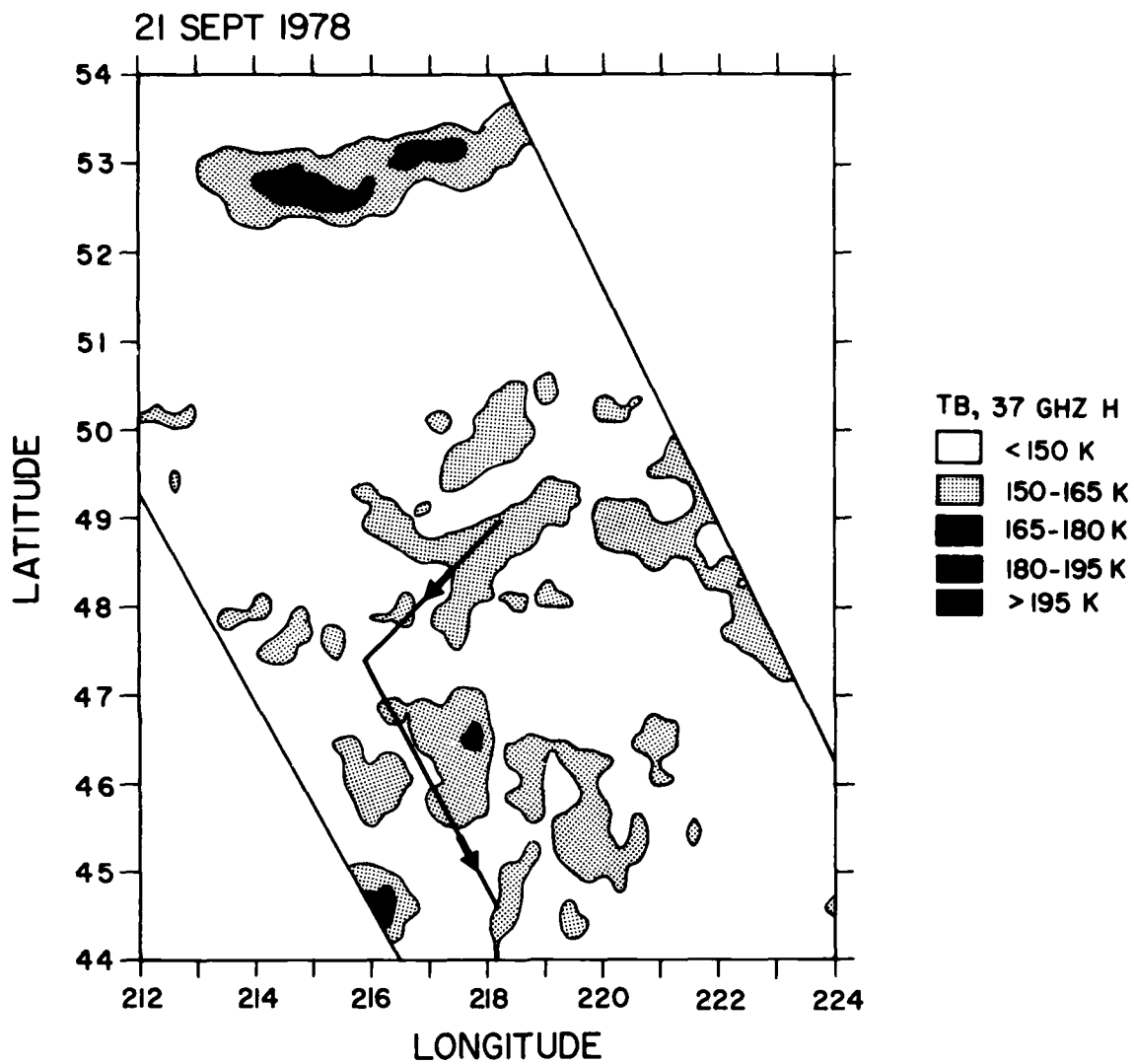
26

Figure 16.   Contour map of SMMR T_B at 37 GHz H polarization in the GOASEX area on 21 September 1978 with the aircraft flight track.
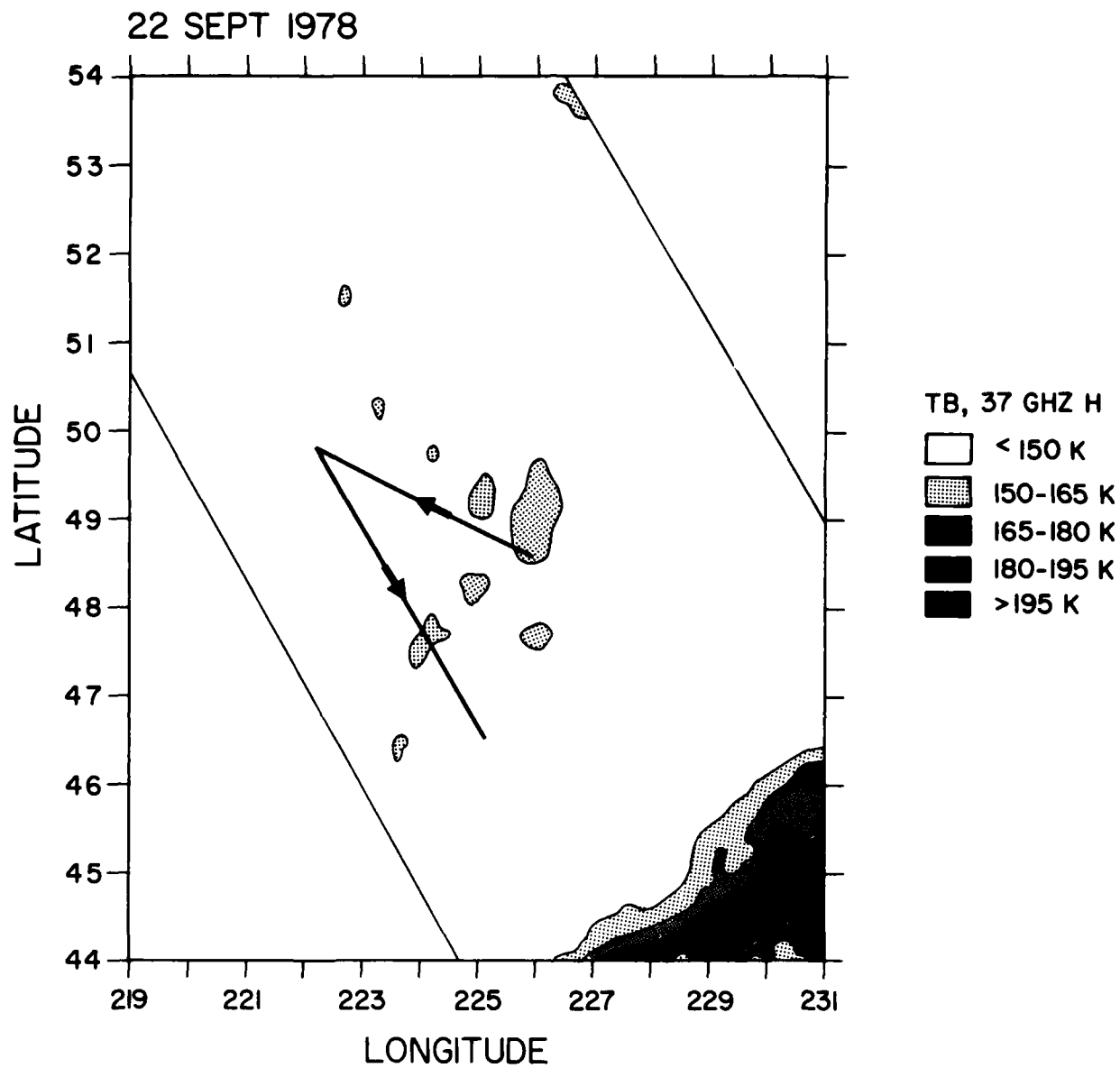
Figure 17. Contour map of SMMR T_B at 37 GHz H polarization in the GOASEX area on 22 September 1978 with the aircraft flight track.

25 SEPT 1978

TB, 37 GHZ H

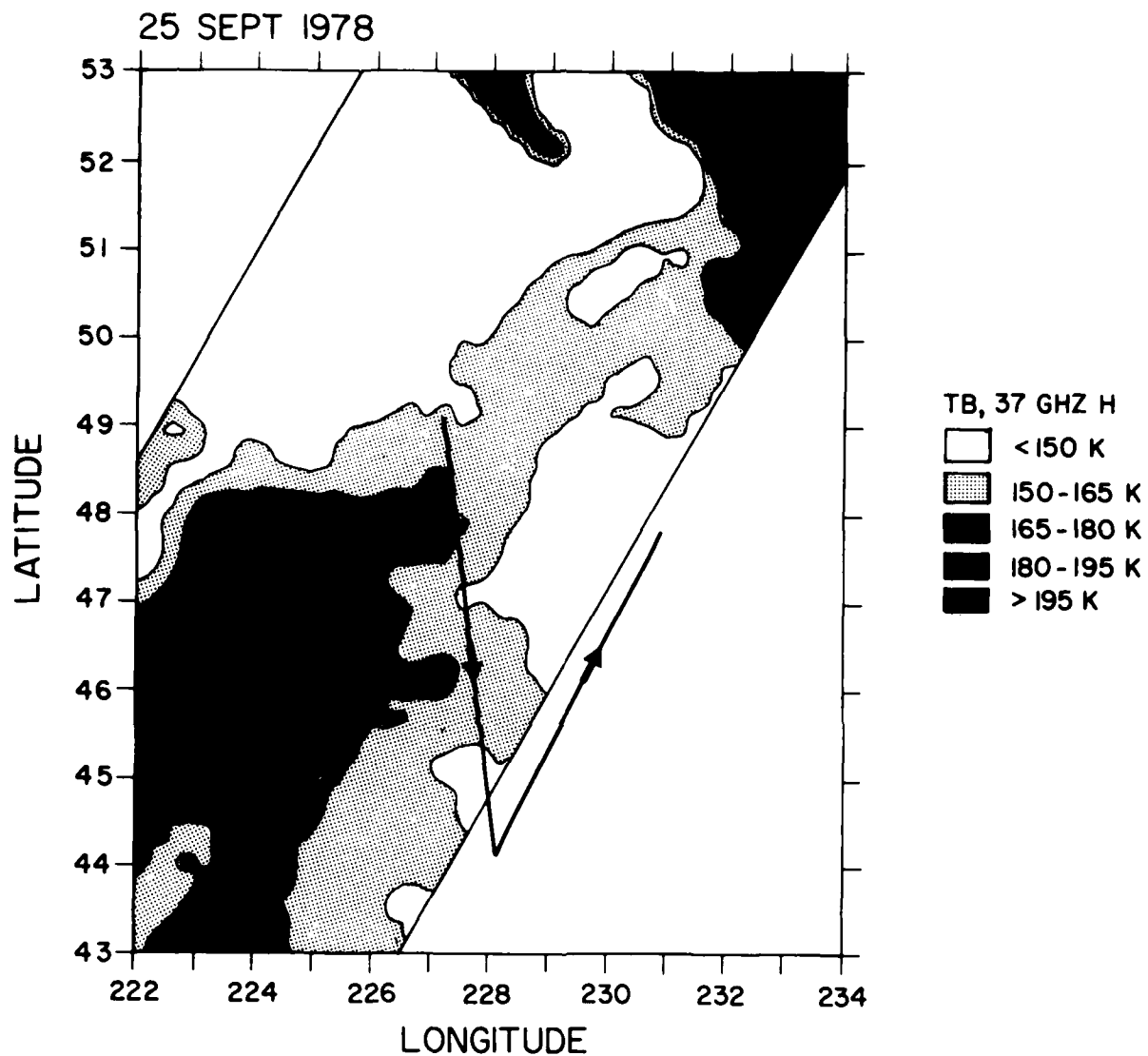|	
☐	< 150 K
▨	150 - 165 K
■	165 - 180 K
■	180 - 195 K
■	> 195 K

LATITUDE

LONGITUDE

Figure 18. Contour map of SMMR T_B at 37 GHz H polarization in the GOASEX area on 25 September 1978 with the aircraft flight track.
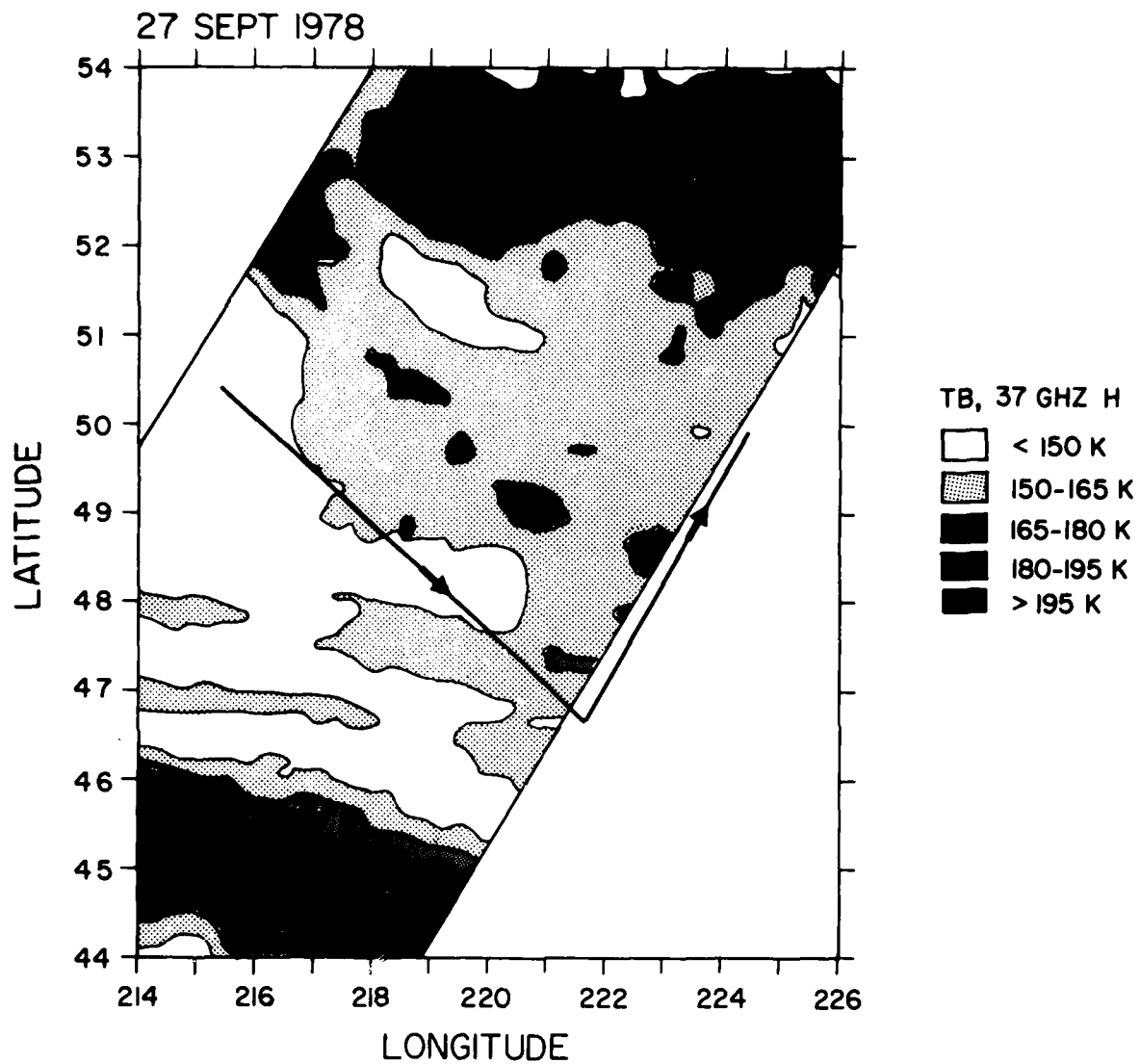
29

Figure 19. Contour map of SMMR T_B at 37 GHz H polarization in the GOASEX area on 27 September 1978 with the aircraft flight track.

where C refers to the value of T_B computed from the NRL Environmental Model. The calculated difference in T_B is 2 K or less.

B. <u>Frequency</u> - The results of (A) are used to obtain an estimate $E(F_S,48.8,\text{low})$ of T_B at SMMR frequency, F_S, and aircraft altitude. Figure 20 shows an example of computed T_B versus frequency for both V and H polarization with the location of all SMMR and aircraft frequencies. The T_B curves are computed for aircraft altitude, 48.8° incidence angle, and for meteorological conditions of the 22 September flight, and are shown simply to illustrate the relative SMMR and aircraft frequencies and the expected T_B differences between the two sets of frequencies. Obviously, T_B at a given F_S can be derived sometimes by extrapolation from a nearby F_A and sometimes by interpolation between two frequencies F_{A1} and F_{A2}. For extrapolation,

$$E(F_S,48.8,\text{low}) = E(F_A,48.8,\text{low}) + [C(F_S,48.8,\text{low})$$
$$- C(F_A,48.8,\text{low})] \tag{6A}$$

For interpolation,

$$E(F_S,48.8,\text{low}) = fE(F_{A1},48.8,\text{low}) + (1-f)\ E(F_{A2},48.8,\text{low}) \tag{6B}$$

where

$$f = \frac{C(F_{A2},48.8,\text{low}) - C(F_S,48.8,\text{low})}{C(F_{A2},48.8,\text{low}) - C(F_{A1},48.8,\text{low})} \ .$$

C. <u>Altitude</u> - The results of (B) are extrapolated to the satellite altitude, i.e., the low altitude estimate $E(F_S,48.8,\text{low})$ is used to derive the high altitude estimate $E(F_S,48.8,\text{high})$ for direct comparison with the SMMR measurements:

$$E(\text{high}) = L(\text{low,high})\ E(\text{low}) + T_{up}(\text{low, high}) \tag{7}$$

where L is the atmospheric loss factor and T_{up} is the upwelling atmospheric radiation between the two altitudes. The arguments F_S and 48.8, which are common to all terms in equation (7), have been dropped. L and T_{up} are calculated by the Environmental
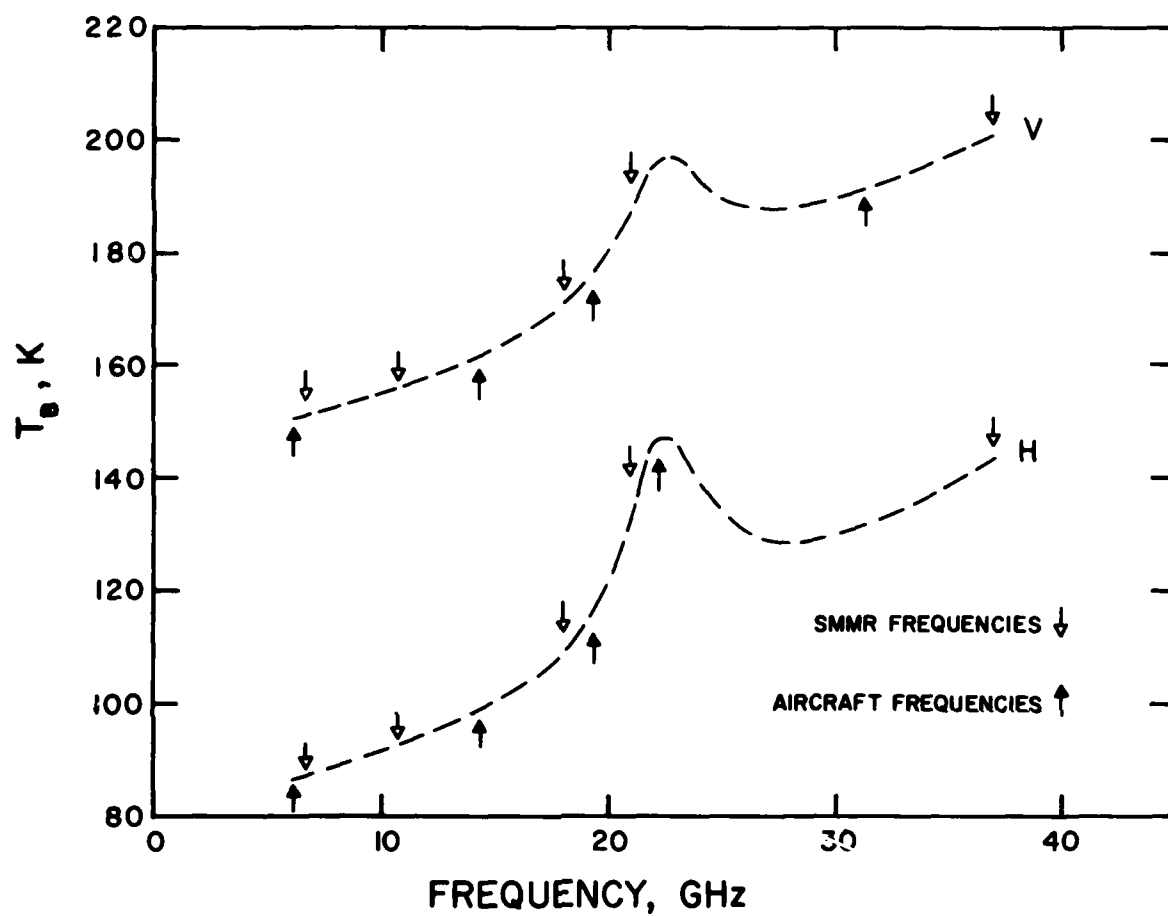
Figure 20.   Sample brightness temperature curves illustrating
              the relative position of the SMMR frequencies and
              the aircraft frequencies.

Model. The resulting estimated increase in T_B due to altitude extrapolation, E (high) - E (low), varies from approximately 2 K at 6.63 GHz to 12 K (clear sky) or 21 K (cloudy sky) at 37 GHz.

When equations (5) - (7) are combined, we obtain the esti-mate $E(F_S, 48.8, high)$ as a linear function of the measurements $M(F_A, 50, low)$. Only one measurement is involved when frequency extrapolation is used,

$$E(F_{S)}, 48.8, high) = a_1 M(F_A, 50, low) + a_2, \qquad (8)$$

but two measurements are necessary for interpolation,

$$E(F_{S)}, 48.8, high) = a_1 M(F_{A1}, 50, low) + b_2 M(F_{A2}, 50, low) + b_3. \qquad (9)$$

The terms a_1, a_2, b_1, b_2, and b_3 depend only on the Environmen-tal Model calculations and are totally independent of the measured aircraft brightness temperatures.

As seen in Figure 20, most of the SMMR frquencies are close enough to one of the aircraft frequencies that the T_B estimate can be extrapolated from a single aircraft measurement according to equation (8). An exception is the SMMR frequency 10.69 GHz, which lies intermediate between the aircraft frequencies 6.15 and 14.3 GHz. Consequently, the T_B estimate for 10.69 GHz is derived from the aircraft measurements at 6.15 and 14.3 GHz by interpolation according to equation (9). Also, the SMMR 37 GHz is far removed from the closest aircraft frequencies of 22.2 GHz (H polarization) and 31.3 GHz (V polarization), so that there will be more uncertainty in the resulting T_B estimates at 37 GHz than those at any of the other SMMR frquencies. Table 3 lists the SMMR frequencies, the corresponding aircraft frequencies, and the methods used in deriving the T_B estimates.

TABLE 3

SMMR and Aircraft Frequencies and Polarization

SMMR		Aircraft
6.63 v	Extrapolation	6.15 V
6.63 H		6.15 H
10.69 V	Interpolation	6.15 V and 14.3 V
10.69 H		6.15 H and 14.3 H
18 V	Extrapolation	19.3 V
18 H		19.3 H
21 V	Extrapolation	19.3 V
21 H		19.3 H
37 V	Extrapolation	31.3 V
37 H		22.2 H

4.0 RESULTS

A total of eight separate locations are selected from the four flights for T_B comparisons. These locations include the four star-pattern areas. The other four locations are chosen near the center of the SMMR swath where polarization angle α is close to zero and cross-polarization errors are consequently minimized. Table 4 lists for each location the latitude, longitude, date, and time at which the aircraft measurements were made. For the star patterns, which took approximately one hour, the mid-time and mid-location are given.

TABLE 4

SMMR/Aircraft T_B Comparison Locations

Date	GMT	North Lat.	East Long.	SEASAT Pass No.	SEASAT Overpass Time
21 Sept	1800	49.0	218.3	1241	1852
21 Sept	1854	48.4	217.2	1241	1852
22 Sept	1650	48.7	226.3	1255	1822
22 Sept	1736	48.9	225.3	1255	1822
22 Sept	1827	49.7	222.3	1255	1822
25 Sept	0620	48.9	226.8	1292	0850
27 Sept	0650	50.3	215.3	1321	0931
27 Sept	0810	48.5	218.7	1321	0931

The brightness temperatures at aircraft altitude are averaged for the eight locations and plotted versus frequency in Figures 21-23 for H polarization, V polarization, and the sum of H and V. Table 5 lists the averaged values for H and V. Theoretical brightness temperatures are calculated for each case by the Environmental Model, averaged, and also shown. Two sets of environmental calculations are made, one set assuming no clouds and the other set assuming complete cloud cover, i.e., representing minimum or maximum cloud effect on T_B. Figures 21-23 show that there is reasonable agreement between the aircraft measurements and theory. An exception is that there is better agreement for H + V than for H or V individually at 6.15 and 14.3 GHz, indicating the possibility of some depolarization error at these two frequencies.

TABLE 5

Brightness Temperatures at Aircraft Altitude

	Aircraft T_B, K	
Frequency, GHz	H	V
6.15	88.2	148.8
14.3	98.9	156.9
1ɔ.3	111.4	175.6
22.2	141.7	–
31.4	–	194.1

The eight sets of aircraft measurements are then extrapolated to SMMR angle, frequency, and altitude according to the previously outlined method to obtain estimates of SMMR T_B's. The calculations are performed twice, assuming first no clouds and then assuming clouds. This method results in a spread in the estimated SMMR T_B's. The actual SMMR measurements should fall within this range, since the large SMMR footprints are likely to be partly cloud-filled and partly clear. Figures 24-26 show the averaged estimated SMMR T_B's for H polarization, V polarization, and the sum of H and V. Note that the relation between the aircraft measurements and theory at aircraft altitude seen in Figures 21-23 is preserved in the relation between the
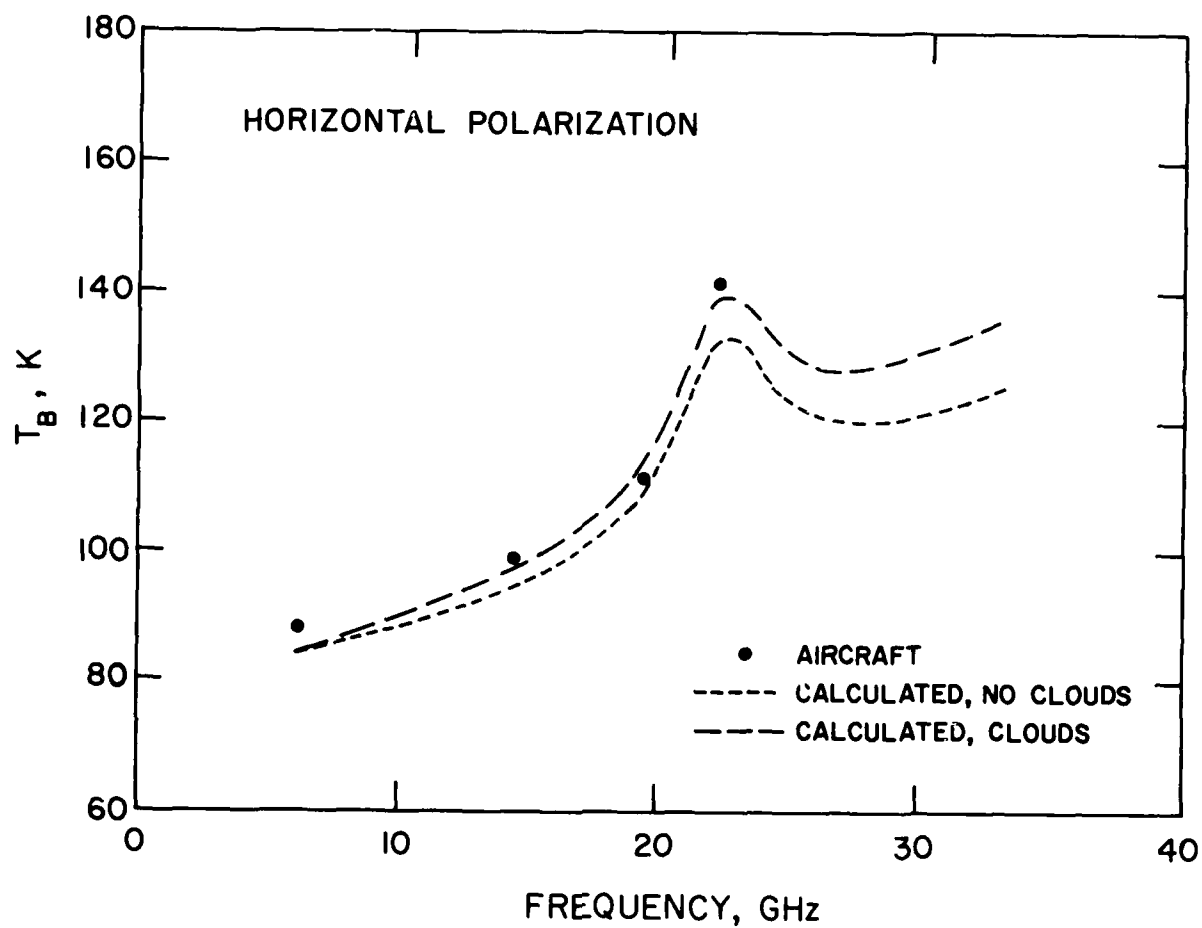
Figure 21. Measured aircraft T_B and calculated T_B for H polarization at aircraft altitude, averaged over eight locations.
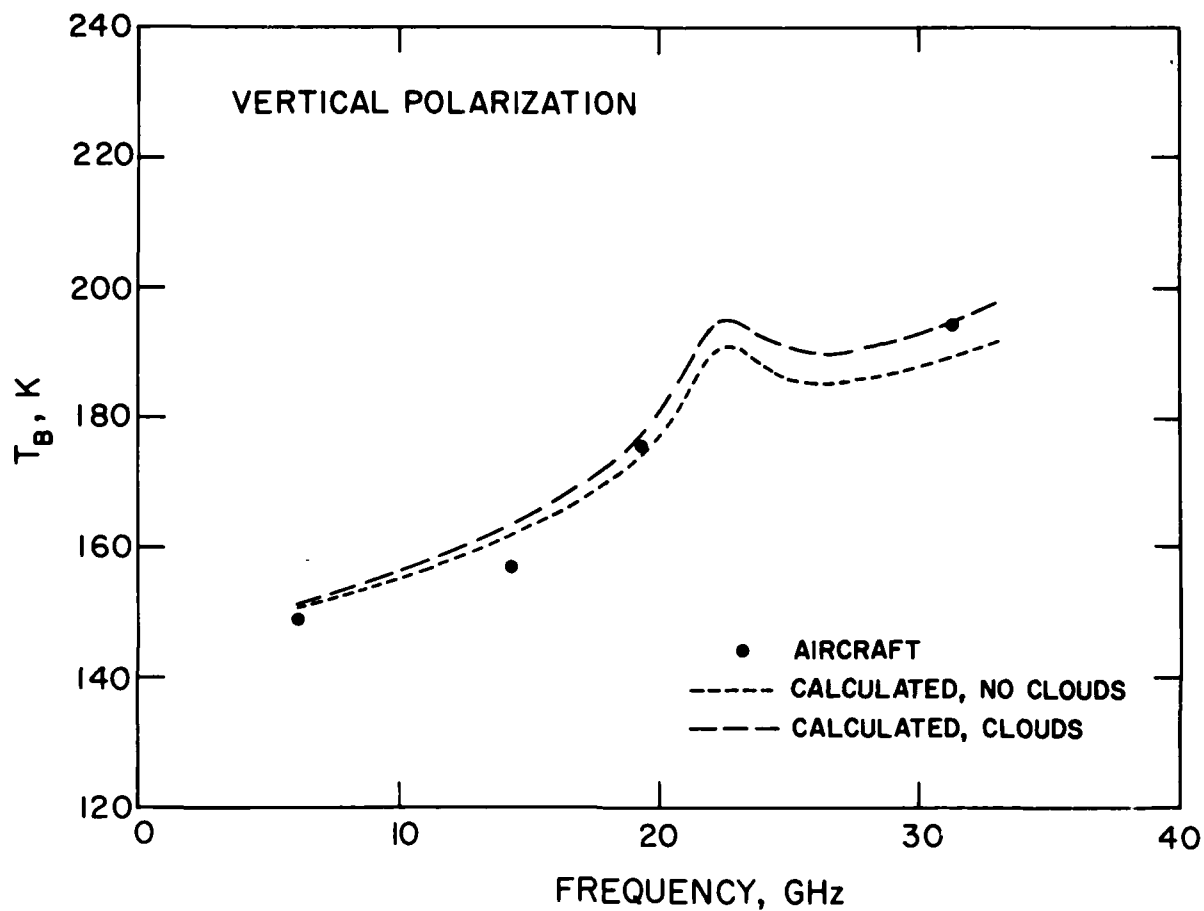
Figure 22. Measured aircraft T_B and calculated T_B for V polarization at aircraft altitude, averaged over eight locations.
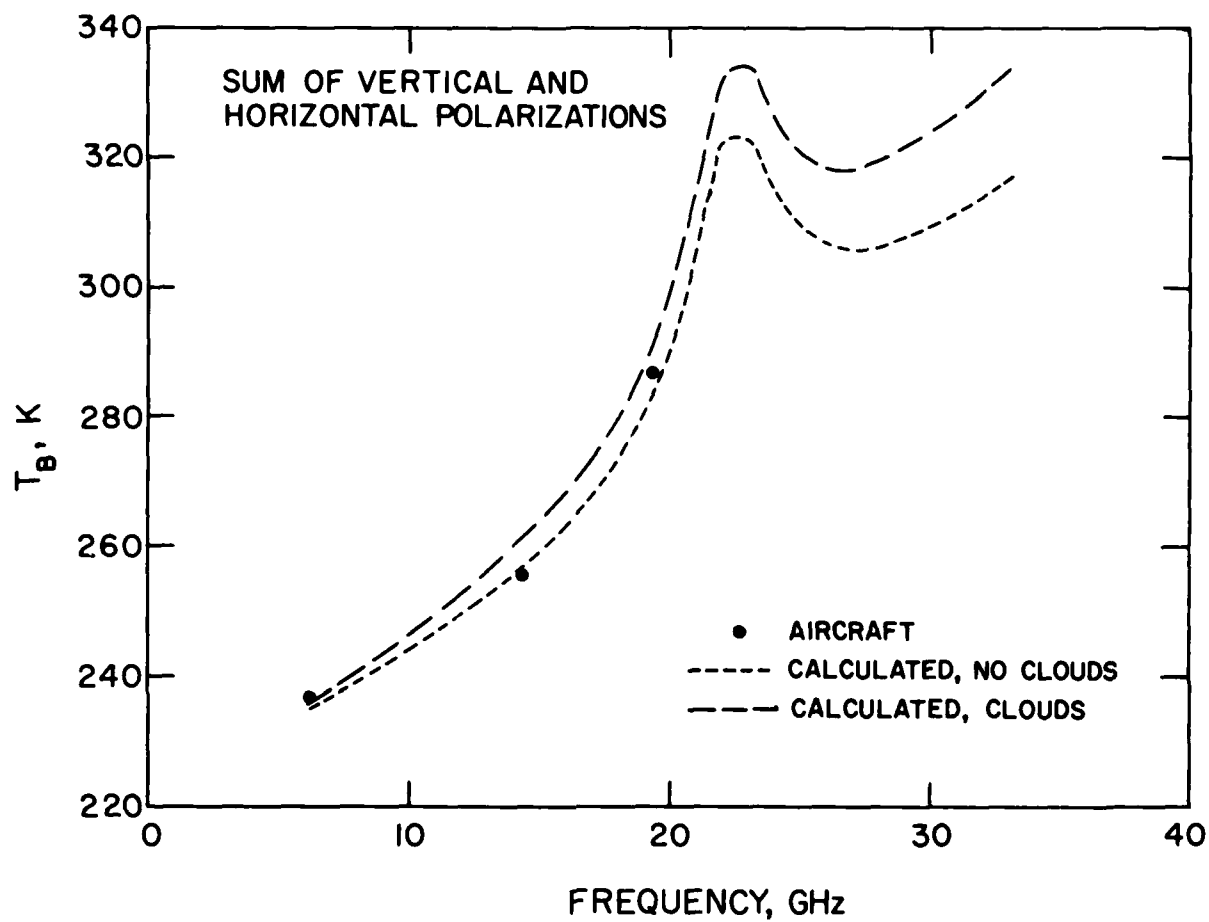
Figure 23. Measured aircraft T_B and calculated T_B for sum of V and H polarizations at aircraft altitude, averaged over eight locations.

estimated SMMR T_B's and theory at satellite altitudes seen in Figures 24-26. This result indicates that the extrapolation of the aircraft measurements from aircraft conditions to satellite conditions is being performed correctly.

Next, the actual SMMR measurements for the eight locations are determined, averaged, and plotted in Figures 24-26. The SMMR T_B's in the star areas are determined by averaging all SMMR measurements occuring within the region covered by the RP-3A in flying the star pattern. For the non-star locations, the SMMR measurements are averaged in square areas around the locations, the size of the square being 20 km for 37 GHz, 60 km for 6.63 GHz, and 35 km for all other frequencies. The sizes of the squares are chosen so that a minimum of two SMMR measurements are averaged at each location for each frequency.

Figures 24-26 show that the SMMR T_B's are generally low compared to the estimates derived from the aircraft measurements, except at 6.63 GHz H and V and at 21 GHz H. The aircraft measurements and the theory are comparatively consistent, especially in the H + V curve of Figure 26, where depolarization errors are nullified. It must be concluded that there are significant errors in the measured SMMR brightness temperatures at most frequencies.

Table 6 summarizes the data shown in Figures 24 and 25; the aircraft T_B is the average of the two values for clouds and for no clouds. The resulting bias, listed in the last column of Table 6, is the amount which must be added to the SMMR T_B to bring it into agreement with the aircraft T_B. Most of the bias values are greater than 5 K, i.e., significa...ly large.
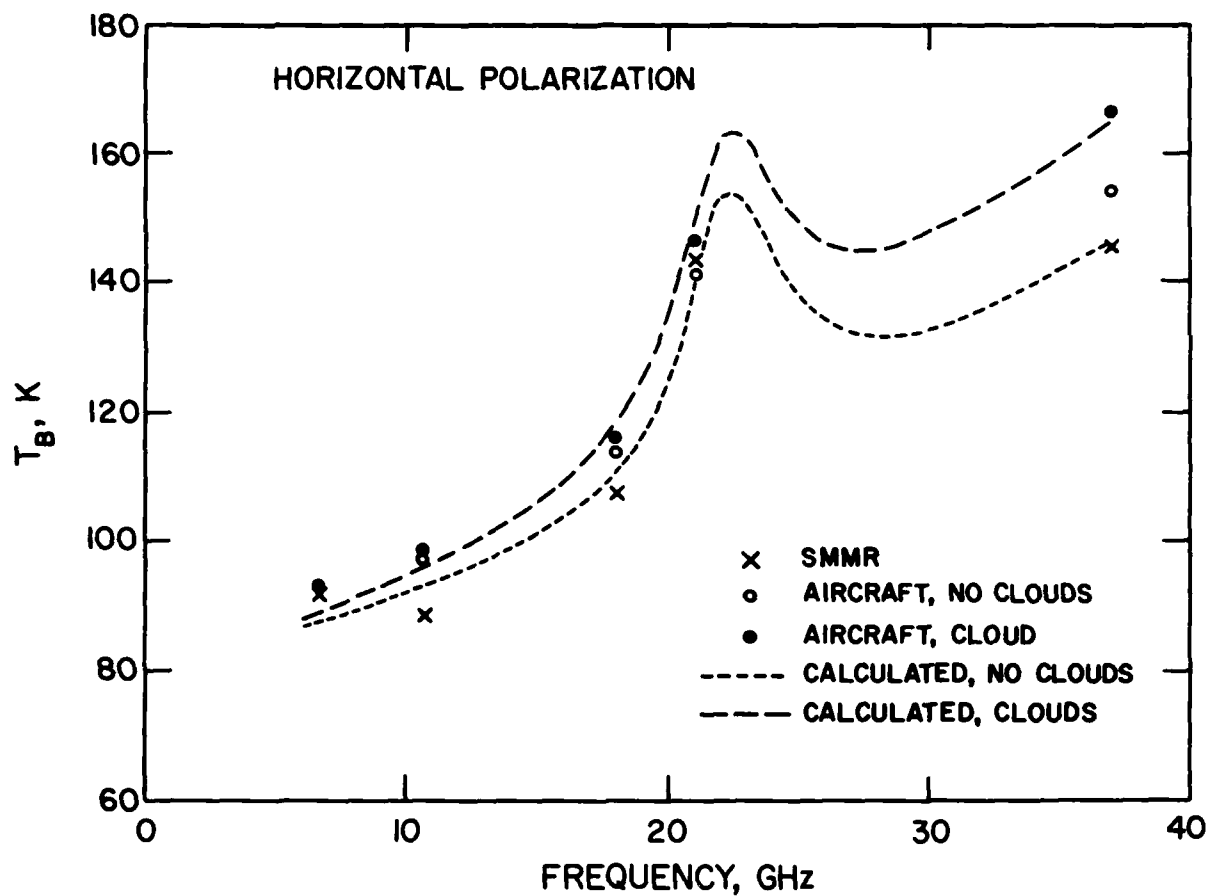
Figure 24. Measured SMMR T_B, estimated SMMR T_B from aircraft measurements, and calculated T_B for H polarization at satellite altitude, averaged over eight locations.
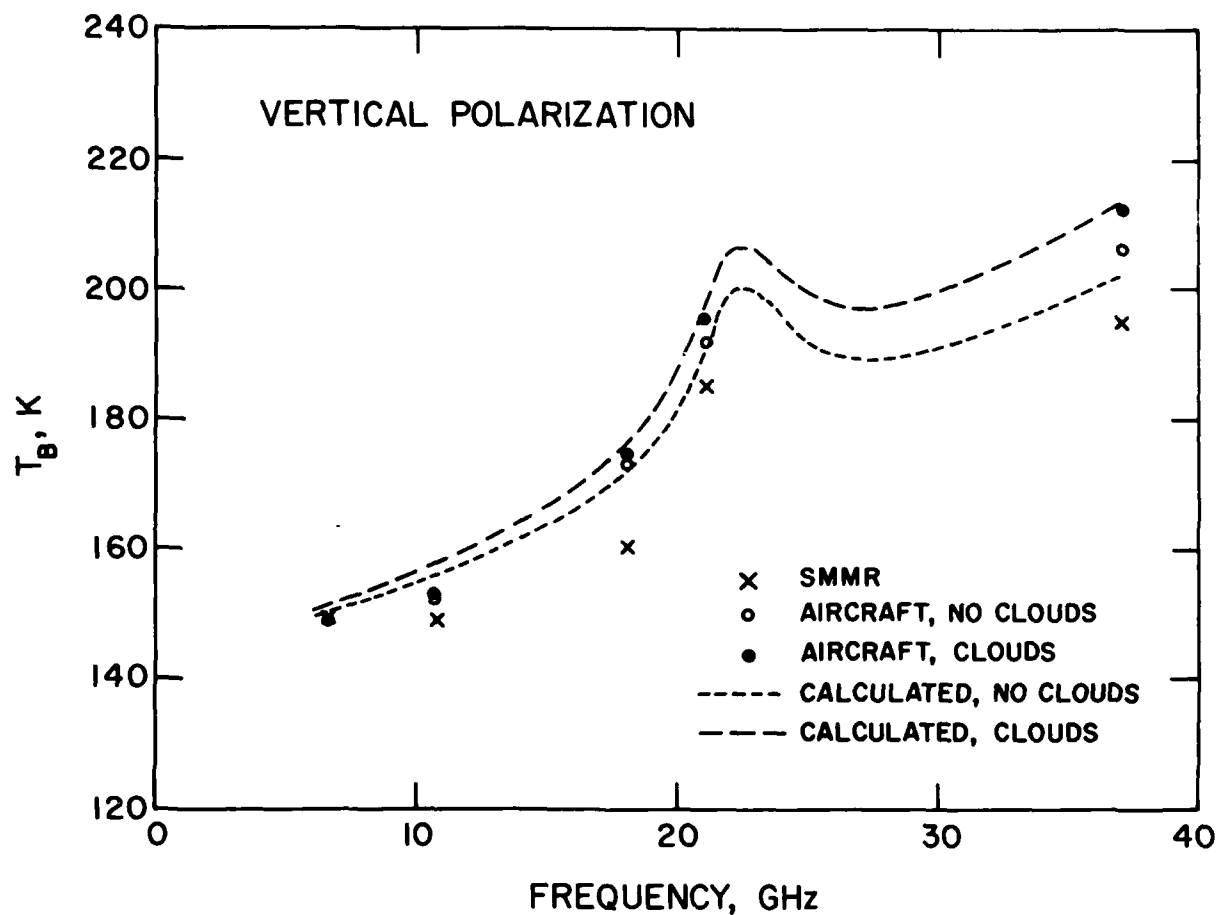
Figure 25. Measured SMMR T_B, estimated SMMR T_B from aircraft measurements, and calculated T_B for V polarization at satellite altitude, averaged over eight locations.
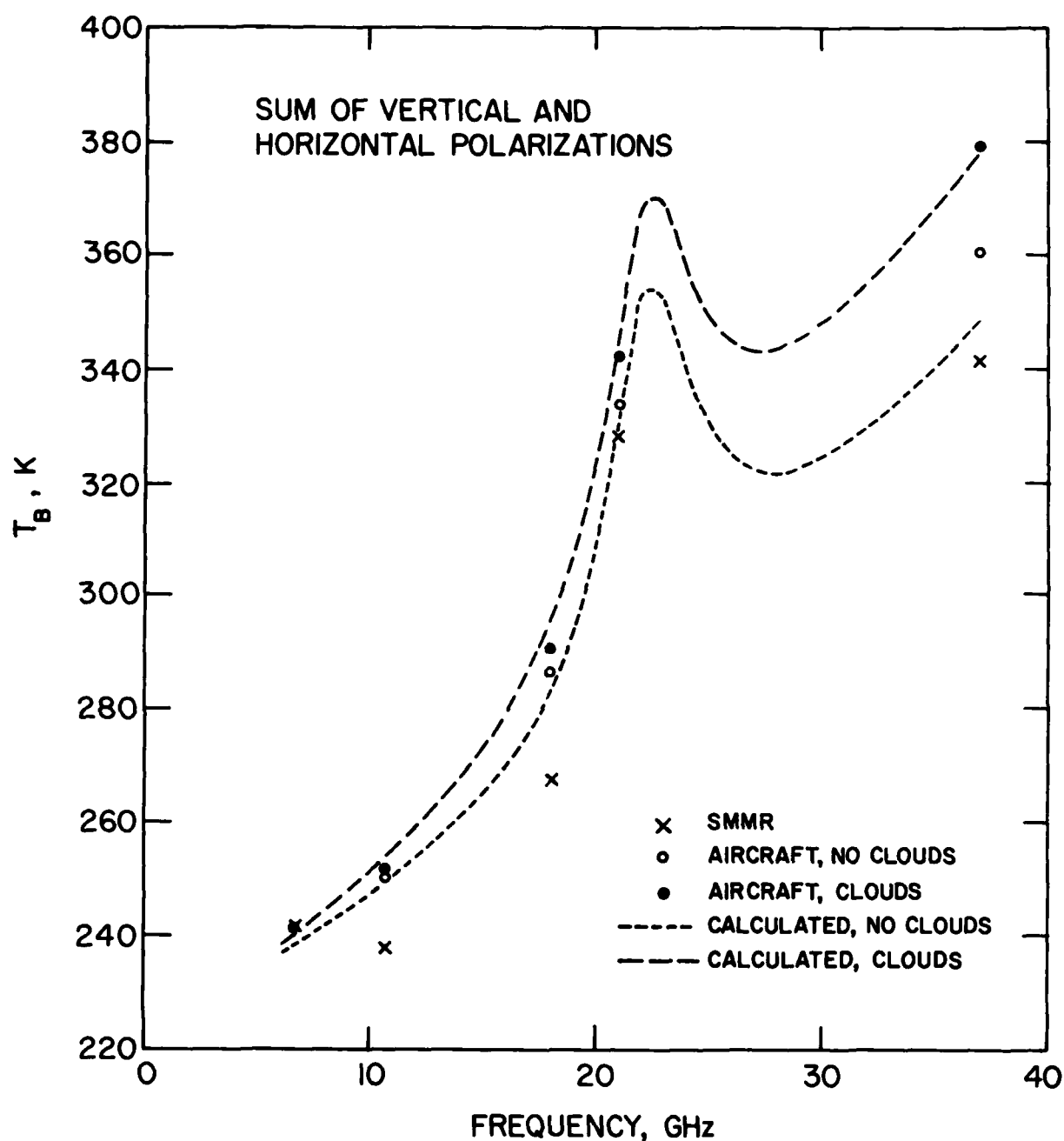
Figure 26. Measured SMMR T_B, estimated SMMR T_B from aircraft measurements, and calculated T_B for sum of V and H polarization at satellite altitude, averaged over eight locations.

TABLE 6

Brightness Temperatures from SMMR and Aircraft at SFASAT Altitude

	SMMR T_B, K	Extrapolated Aircraft T_B, K	Bias, K
6.63 H	92.0	92.5	0.5
6.63 V	149.2	148.7	-0.5
10.69 H	88.4	98.2	9.8
10.69 V	149.4	152.8	3.4
18 H	107.4	114.7	7.3
18 V	160.2	173.8	13.6
21 H	143.0	143.8	0.8
21 V	184.6	193.7	9.1
37 H	145.9	160.6	14.7
37 V	194.8	2C9.2	14.4

The SMMR T_B's are used as inputs to various geophysical algorithms for the retrieval of geophysical parameters such as sea surfaces temperature (SST) and ocean wind speed. Incorrect T_B values will result in the production of incorrect geophysical parameter values from the algorithms. Two methods have been used to compensate for this problem: (1) adding a predetermined bias to correct the SMMR T_B's before using them in the algorithm, or (2) adding a predetermined bias to correct the geophysical parameter after retrieval by the algorithm. In the Wentz geophysical algorithm, the first method is used. The SMMR T_B biases derived here and listed in Table 6 may be compared to recent values used in the Wentz algorithm (Wentz, F.J., private communication). The two sets of biases are plotted in Figure 27. They are in reasonable agreement and the frequency dependence is identical. An exception is that the NRL bias values at 37 GHz are much greater than the corresponding Wentz values, possibly because the NRL values are based on measurements at the much lower frequencies of 22 and 31 GHz.

The results of this report provide independent experimental verification, both qualitatively and quantitatively, of the empirical observation that the brightness temperatures measured by the SEASAT SMMR are in error at most frequencies.
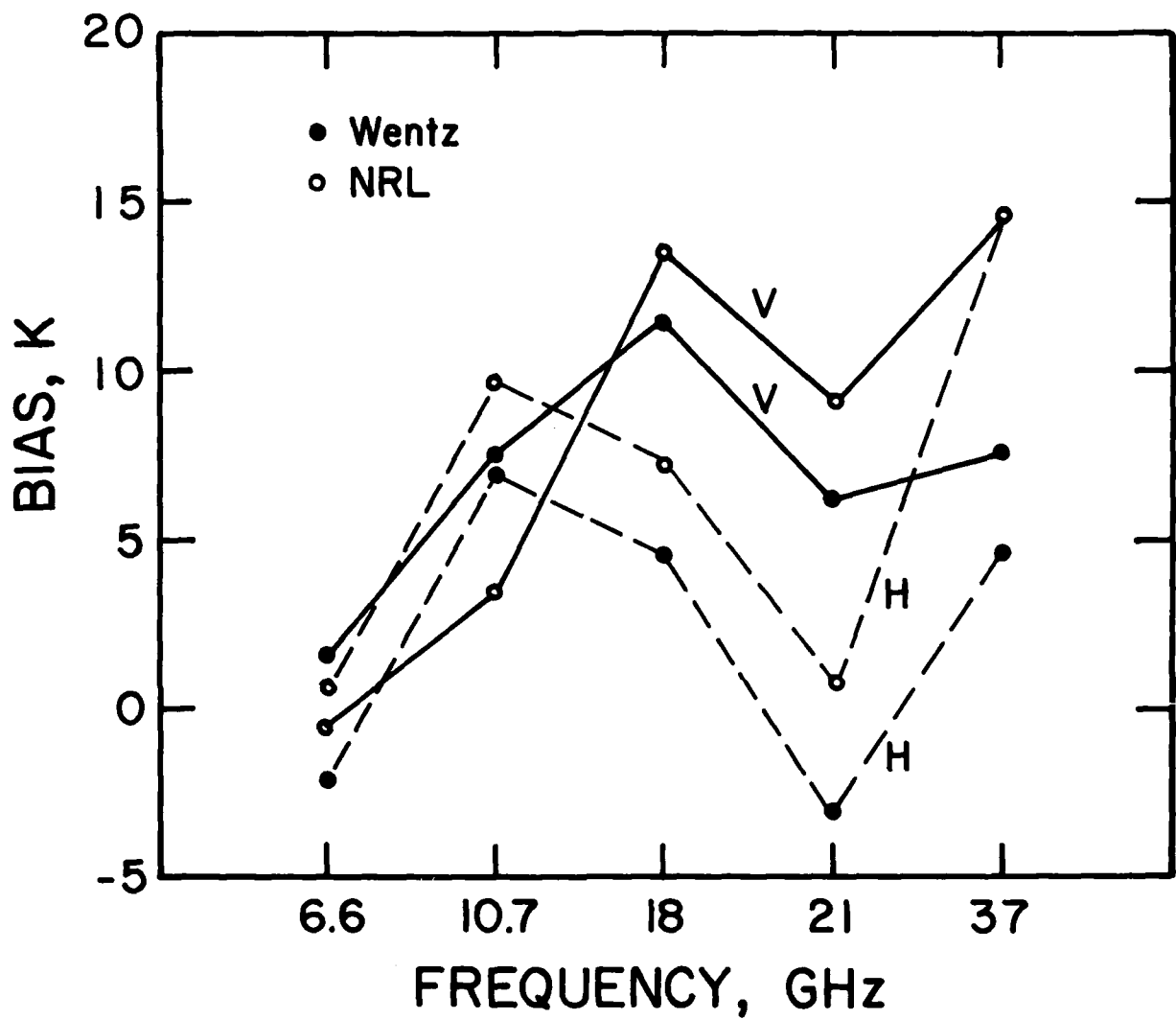
Figure 27. SMMR Bias values, determined experimentally (NRL) and empirically (Wentz).

REFERENCES

Christensen, E.J., in SMMR Mini-Workshop IV Report, JPL
    Internal Document 622-234, 1981.

Claassen, John P., and Adrian K. Fung, The Recovery of Polarized
    Apparent Temperature Distributions of Flat Scenes from
    Antenna Temperature Measurements, IEEE Trans. Antennas
    Propagat., AP-22, 433-442, 1974.

Njoku, Eni G., Edward J. Christensen, and Richard E. Cofield,
    The SEASAT Scanning Multichannel Microwave Radiometer
    (SMMR): Antenna Pattern Corrections-Development and
    Implementation, IEEE J. Oceanic Eng., OE-5, 125-137, 1980a.

Njoku, Eni G., J.M. Stacey, and Frank T. Barath, The Seasat
    Scanning Multichannel Microwave Radiometer (SMMR):
    Instrument Description and Performance, IEEE J. Oceanic
    Engr., OE-5, 100-115, 1980b.

Wisler, M.M., and J.P. Hollinger, Estimation of Marine
    Environmental Parameters Using Microwave Remote Sensing
    Systems, NRL Memo. Rpt. 3661, Naval Research Laboratory,
    Washington, DC, 1977.

END

FILMED

12-83

DTIC